

# The Ultimate Noise Limit for Hall Plates in Voltage, Current, and Hybrid Operating Modes

Udo Ausserlechner

Department Sense and Control, Infineon Technologies AG, Villach, Austria

Email: udo.ausserlechner@infineon.com

**How to cite this paper:** Ausserlechner, U. (2020) The Ultimate Noise Limit for Hall Plates in Voltage, Current, and Hybrid Operating Modes. *Journal of Applied Mathematics and Physics*, 8, 3019-3059. <https://doi.org/10.4236/jamp.2020.812223>

**Received:** November 27, 2020

**Accepted:** December 21, 2020

**Published:** December 24, 2020

Copyright © 2020 by author(s) and Scientific Research Publishing Inc. This work is licensed under the Creative Commons Attribution International License (CC BY 4.0).

<http://creativecommons.org/licenses/by/4.0/>



Open Access

## Abstract

If Hall plates are used as magnetic field sensors they are usually powered up by a current source connected to a pair of non-neighboring contacts. The output voltage is tapped at another pair of non-neighboring contacts. In this paper we study more general operating conditions of Hall plates with an arbitrary number of contacts. In such hybrid operating modes current sources are connected to a first set of contacts and voltage sources to a second set of contacts. Output voltages are tapped at the first set of contacts and output currents are measured at the second set of contacts. All these output signals are multiplied by coefficients and added up. The purpose of this work is to figure out which operating mode and which Hall plate achieve maximum signal at minimum thermal noise and power dissipation. To this end we develop a theory, which gives the ratio of signal over noise and power as a function of the resistance matrix of Hall plates, of the supply voltages and currents, and of the coefficients. Optimization is done analytically in closed form and numerically for specific examples. The results are: 1) all operating modes have identical noise performance if their parameters are optimized; 2) for any Hall plate one can measure its resistance matrix and insert its values into our formulae to obtain the optimum supply currents and coefficients for optimum noise performance.

## Keywords

Canonical-Correlation Analysis, Fractional Programming, Hybrid  $N$ -Pole Matrix, Multi-Port Hall Plates, Noise Efficiency, Rayleigh Quotient, Signal to Noise Ratio

## 1. Introduction

In this work we study different ways of how to supply Hall plates with d.c. electric energy and how to extract signals from them. The goal is to construct signals

with maximum sensitivity to impressed magnetic field and minimum thermal noise at lowest possible electric power dissipation. Thus, we look for maximum signal to noise (*SNR*) at given power. Thereby we focus on the *circuit* into which the Hall plate is embedded, irrespective of the specific shape of the Hall plate itself. For any kind of Hall plate there should be a specific circuit which optimizes the *SNR*. What is the topology of this optimum circuit and how can we find its optimum parameters for a given Hall plate?

Thereby the Hall plates are allowed to be as general as possible: we only require that their voltages and currents are linked via a matrix, whose elements are constant with respect to voltages and currents. In other words, we assume electrical linearity, which implies no self-heating, no velocity saturation, no junction-field effect [1]. The contacts must be perfectly conducting and ohmic. The current density in the Hall plate must be low enough for its accompanying magnetic field to be negligible to the externally applied magnetic field, *i.e.*, no magnetic self-field effects [2] [3] [4]. Yet anisotropy and inhomogeneity of conductivity and magnetic field are allowed [5] [6]. The Hall plates do not necessarily have to be plates with thin plane geometry. They can also be 3D-shells [7]. They also do not necessarily have to be single connected regions and the contacts may be peripheral or inside the Hall region [8]. The number of contacts is three or larger, and their size can be point-sized or extended. Also Vertical Hall effect devices are within the scope of this paper [9] [10] [11]. Some Hall effect devices consist of several disjunct Hall effect regions connected with wires [12]—our theory also applies to them. It is also allowed for Hall effect devices to have contacts which are not connected, like e.g. the floating buried layer in Vertical Hall effect devices in BiCMOS technologies [12]. The shapes of the Hall effect regions do not need to have any kind of symmetry, although in practice, symmetry generally helps to improve overall performance.

Our general theory builds upon the resistance matrix of an arbitrary Hall effect device. One can either measure it or compute it like shown in [13] [14]. However, there the theory is limited to thin, plane, single connected Hall effect regions with peripheral contacts. Although these are no severe restrictions for practical use, it rules out some “exotic” variants like [15] [16] [17] [18]. The formulae of [14] apply for circular Hall plates. Yet, this shape is no real limitation, because it is possible to map any other single connected plane region via conformal transformation onto the circular shape [19]. According to Wick, this transformation does not change the resistances, currents, and voltages seen at the contacts [20]. Also thermal noise and power dissipation are invariant to conformal transformation. On the other hand, local quantities like electric field, current density, power density, 1/f-noise, and self-heating will not be constant under a general conformal transformation, but these quantities are irrelevant in a first order linear theory of Hall plates.

A major source of error in Hall plates is the zero-point error, also called offset error. Luckily, it is possible to eliminate offset errors in Hall plates with linear electric behavior. This is a consequence of the principle of reverse magnetic field

reciprocity (RMFR) [21] [22], which follows from Onsager's reciprocity principle [23]. Practical implementations are known as contact commutation schemes or spinning current schemes [12] [24] [25].

A nice feature of spinning current schemes is that they also eliminate low frequency noise ( $1/f$ -noise) [26] [27]. Therefore the dominant noise source in spinning current circuits for Hall plates of typical sizes greater than  $10\ \mu\text{m}$  is thermal noise. In this work we focus on the ratio of the Hall output signal over the thermal noise, which we call *SNR*.

In a preceding work we have shown that the *SNR* of Hall plates can be improved by up to 90% over conventional Hall plates with four contacts [25]. These new Hall plates must have many contacts, all of which are supplied by current sources and tapped by voltmeters, and the circuit has to sum up all voltage readings to obtain an overall output signal. We call this method the *voltage mode operation*, because voltage is measured. Note that we measure voltage at *all* contacts and therefore it does not make sense to supply any contacts with voltage sources. Then, the only meaningful way to operate the Hall plate is to supply all its contacts with current sources, albeit some of them may supply zero current.

The starting question for this paper was to show, that for identical power, the *SNR* of Hall plates in voltage mode operation is identical to the *SNR* in *current mode operation*. With current mode operation we mean that voltages are supplied to the contacts of a Hall plate and output currents are measured at *all* contacts. We will prove this hypothesis at weak magnetic field.

Naturally, the equivalence of voltage and current mode operation leads to the question, how mixed modes of operation behave. Voltage and current mode are just specific cases of these more general *hybrid operating modes*. Thus, one may ask, if voltage and current mode are the best out of all hybrid modes. This is all the more interesting with regard to the considerable number of hybrid modes: a Hall plate with 10 contacts has  $2^9 = 512$  hybrid operating modes.

In **Section 2** we describe three types of Hall sensor circuits. **Section 3** gives a definition of the signal-to-noise ratio (*SNR*) and the noise efficiency. It also explains the difference in power dissipated in the Hall plate and in the total circuit. The basic scheme of how to describe hybrid operating modes is worked out there. In **Section 4** the formulae are derived for the *SNR* at weak magnetic field, and **Section 5** gives numerical examples of how to use the theory. **Section 6** explains that the maximum *SNR* over power is related to the largest eigenvalue of a matrix, and how this matrix is related to the resistance matrix of the Hall plate. **Appendix A** gives a short introduction to the gyrator. **Appendices B, C, and D** prove some properties of matrices used in the theory.

## 2. Circuits for Multi-Contact Hall Plates

We consider circular Hall plates with  $N$  contacts, where  $N$  is an even or odd integer number greater than 2 (see **Figures 1-3**). All contacts are labelled in

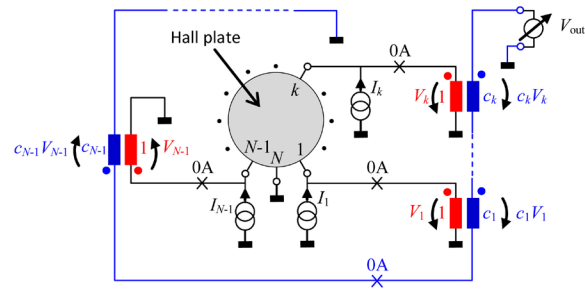


**Figure 1.** Hall plate with  $N$  contacts in a conceptual circuit for *voltage mode operation*. Current sources at the contacts supply the Hall plate with electric energy. The  $N$ -th contact is at reference potential.  $N - 1$  passive noise-less ideal transformers tap the potentials at the contacts. Each transformer has a dedicated turns ratio  $1:c_k$ . The secondary sides of all transformers are connected in series to add up all output voltages. This sum is measured by an ideal voltmeter with infinite impedance.

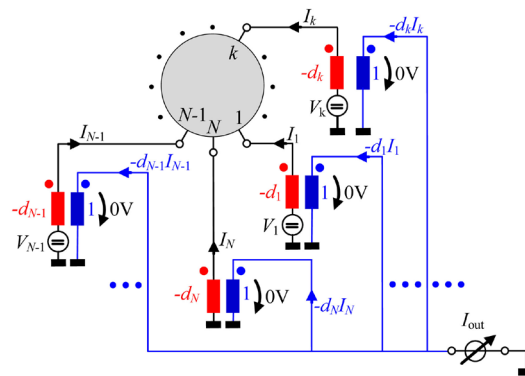


**Figure 2.** Hall plate with  $N$  contacts in a conceptual circuit for *current mode operation*. Voltage sources at the contacts supply the Hall plate with electric energy. The  $N$ -th contact is at reference potential.  $N$  passive noise-less ideal transformers tap the currents through the contacts. Each transformer has a dedicated turns ratio  $-d_k:1$ . The secondary sides of all transformers are connected in parallel to add up all currents. This sum is measured by an ideal ampere-meter.

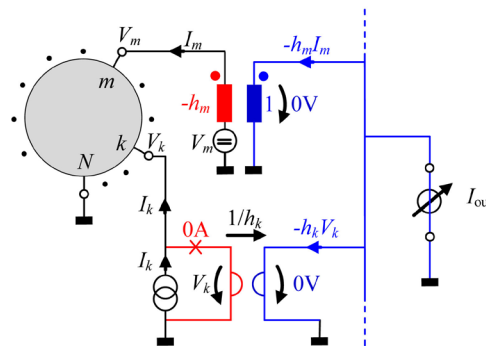


**Figure 3.** Hall plate with  $N$  contacts in a conceptual circuit for *hybrid mode operation*. The Hall plate is supplied with electric energy via voltage sources  $V_m$  and current sources  $I_k$ . If a contact is supplied by a voltage source, current is measured as an output signal via an ideal transformer. If a contact is supplied by a current source, voltage is measured as an output signal via a gyrator. The outputs of all ideal transformers and gyrators are summed up to  $I_{out}$  and measured by an ampere-meter. The turns ratios of the transformers is  $-h_m:1$  and the trans-resistance of the gyrators is  $1/h_k$ .

sequential order along the periphery. The  $N$ -th contact is grounded. In general, the contacts are irregular in size and position.

We consider various operating modes for multi-contact Hall plates. In *voltage mode operation* the Hall plate is supplied by current sources and its output voltages are measured (**Figure 1**). Conversely, in *current mode operation* the Hall plate is supplied by voltage sources and its output currents are measured (**Figure 2**). Between these two extremes there are numerous *hybrid* cases, where current sources are connected to a first group of contacts while voltage sources are connected to the rest (**Figure 3**). There we measure voltages at the first group of contacts and currents at the rest of the contacts, and we add up these voltages and currents.

## 2.1. A Circuit for Voltage-Mode Operation

Voltage mode operation is shown in **Figure 1**. A Hall plate with  $N$  contacts has  $N-1$  current supplies and  $N-1$  ideal transformers, which tap the output voltage, multiply it by a weighing coefficient  $c_k$  according to the turns ratios, and add up all voltages at the input of the voltmeter. The summing of voltages is done by connecting all secondary coils of the ideal transformers in series.

We use the ideal transformers here only in a conceptual meaning to be able to apply classical theory for passive networks. In a modern circuit one would prefer to use amplifiers instead of transformers. In contrast to real transformers, ideal ones also couple d.c. currents and voltages, *i.e.*, they also work at 0 Hz frequency (their inductance is assumed to be infinite). The ideal voltmeter has infinite impedance. Hence, no current flows through it and through the secondary sides of all ideal transformers. Therefore, also no current flows through the primary sides of all ideal transformers. Consequently, the ideal transformers do not load the Hall plate with current: The currents of all current sources flow strictly into the Hall plate, and not through the ideal transformers. The ideal transformers are passive and lossless, *i.e.*, they do not add or subtract power or noise to the signals. Thus, the *SNR* at the voltmeter comes from the Hall plate only. Voltages are measured with respect to reference potential (=ground). Therefore, it makes no sense to measure the voltage at contact  $N$ , because it is grounded.

The question is, which currents  $I_k$  and which weighing coefficients  $c_k$  maximize the *SNR* at the voltmeter. Obviously, the *SNR* increases if we multiply all currents by a fixed number greater than 1. Thus, for a unique solution we need to normalize the currents:

$$\sum_{k=1}^{N-1} I_k^2 = 1 \quad (1a)$$

If we multiply all weighing coefficients by a single number, this will not change the *SNR*, because signal and noise are affected likewise. Again, for a unique solution of the coefficient vector we need some kind of normalization:

$$\sum_{k=1}^{N-1} c_k^2 = 1 \quad (1b)$$

The normalizations used in (1a, b) differ from the ones in [25], where we

simply set one current and one coefficient equal to 1. However, for general asymmetric Hall plates we do not know, if the current and the coefficient of a particular contact should be zero in the optimum case. Therefore we use the sum of squares in (1a, b).

## 2.2. A Circuit for Current-Mode Operation

Current mode operation is shown in **Figure 2**. A Hall plate with  $N$  contacts has  $N-1$  voltage sources and  $N$  ideal transformers, which tap the output current, multiply it by a weighing coefficient  $d_k$  according to their turns ratios, and add up all currents at the input of the ampere-meter. The currents are summed up by connecting all secondary coils of the ideal transformers in parallel. Since the ideal ampere-meter has zero impedance, no voltage drops over it. Thus, no voltage drops across the secondary coils of the ideal transformers, and therefore also no voltage drops over their primary coils. Consequently, the voltages of the voltage sources are also present at the contacts of the Hall plate—the ideal transformers do not cause any errors in the supply voltages.

Interestingly, in **Figure 2** we have the same number of supplies, but one more ideal transformer than in **Figure 1**. The difference is at the ground node, where we can measure the current at grounded contact  $N$ . According to Kirchhoff's nodal current law the current at contact  $N$  is the negative sum of all other currents. This holds for the Hall signal current but also for the noise current. Therefore it is likely not to improve the  $SNR$ , but we can keep the term for the moment and figure out later, if it is superfluous.

So far we have interpreted the Hall plates in **Figure 1** and **Figure 2** as  $N$ -poles. Yet, we can also interpret them as  $(N-1)$ -ports with all ports having contact  $N$  in common. With the port interpretation it becomes apparent that the measurement of  $I_N$  in **Figure 2** is redundant, because it is simply the return path of all ports.

Again, we have to normalize voltages and coefficients to get unique solutions.

## 2.3. A Circuit for Hybrid-Mode Operation

The hybrid operating mode seems straightforward as far as it is a simple mixture of voltage and current mode operation. Some contacts are supplied by current sources, others by voltage sources. If current is supplied to a contact, we can measure voltage as an output signal, and vice versa. Finally, we have to add output voltages and output currents. In practice we could use operational trans-conductance amplifiers (OTAs) to convert voltages into currents and add up all currents. In classical network theory we use gyrators. **Appendix A** explains important aspects of them, which we will use in the following. **Figure 3** shows the conceptual circuit for the hybrid operating mode, whereby we make use of the port interpretation and skip any measurement at contact  $N$ . An exemplary contact  $m$  is shown, where voltage  $V_m$  is supplied and current  $I_m$  is coupled out with an ideal transformer and fed into an ampere-meter. Another exemplary

contact  $k$  is shown, where current  $I_k$  is supplied and voltage  $V_k$  is coupled out with a gyrator. With its trans-resistance the gyrator transforms a voltage  $V_k$  into a current at its secondary side and feeds it into the ampere-meter. Note that the zero impedance ampere-meter shorts the secondary sides of all transformers and gyrators. Therefore, the gyrator input currents also vanish and the gyrators do not load the Hall plate.

In **Figure 3** the definition of the coefficient vector  $\mathbf{h}$  is peculiar in so far as its elements have the dimension 1 when they relate to a transformer, yet, they have the dimension of a conductance when they relate to a gyrator.

Again we have to normalize the supply quantities and the coefficients.

### 3. The Noise Efficiency of Multi-Contact Hall Plates

#### 3.1. Definitions

In this paper we want to study Hall signals and noise of *irregular* Hall plates. This is in contrast to [25], where we assumed regular Hall plates. The difference is that irregular Hall plates operated in the circuits of **Figures 1-3** have non-vanishing output signals at zero applied magnetic field. In this work we are *not* interested in this offset error—it can be cancelled out with well-known spinning schemes (contact commutation schemes) (see [24] [25]). Therefore, in the following we study signals and noise in a specific circuit, which we call *difference-field circuit* (see **Figure 4**). Thereby we assume two identical Hall plates operated in the very same way. Yet, one Hall plate is subject to positive magnetic field ( $B_{\perp} > 0$ ), and the other one to negative magnetic field ( $-B_{\perp} < 0$ ). Their output signals are subtracted by an additional circuit, which might be analogue or digital. For the sake of convenience we will think of it as a simple subtraction by a digital electronic circuit. For voltage mode operation this difference-field output is

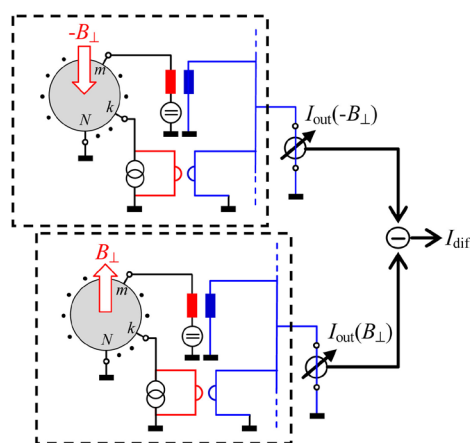


**Figure 4.** Difference-field circuit to study the signal-to-noise ratio of general multi-contact Hall plates. Two identical Hall plates work in identical operating modes yet at different polarity of the applied magnetic field. The circuit inside the two dashed boxes is one of the circuits from **Figures 1-3**. The output signals at both magnetic field polarities  $I_{\text{out}}(+/-B_{\perp})$  are subtracted to give the output  $I_{\text{diff}}$  of the difference-field circuit.

$$V_{\text{diff}} = V_{\text{out}}(B_{\perp}) - V_{\text{out}}(-B_{\perp}). \tag{2a}$$

For the current and hybrid operating modes it is (cf. **Figure 4**)

$$I_{\text{diff}} = I_{\text{out}}(B_{\perp}) - I_{\text{out}}(-B_{\perp}). \tag{2b}$$

At the terminal of  $V_{\text{out}}$  in **Figure 1** a root-mean-squared thermal noise voltage  $v_{\text{out},rms}$  appears, which is related to the output resistance  $R_{\text{out}}$  at this terminal [25]

$$v_{\text{out},rms} = \sqrt{4k_b T R_{\text{out}} ENBW} \tag{3a}$$

with Boltzmann’s constant  $k_b$ , the absolute temperature  $T$ , and the effective noise bandwidth  $ENBW$  of the system. At the terminal of  $I_{\text{out}}$  in **Figure 2** and **Figure 3** a root-mean-squared thermal noise current  $i_{\text{out},rms}$  appears, which is related to the output conductance  $G_{\text{out}}$  at this terminal. It holds  $G_{\text{out}} = 1/R_{\text{out}}$ .

$$i_{\text{out},rms} = \sqrt{4k_b T G_{\text{out}} ENBW} \tag{3b}$$

The reason for choosing ideal transformers and gyrators in the circuits of **Figures 1-3** instead of active circuits like operational amplifiers or trans-conductance amplifiers, is that their output noise is determined merely by  $R_{\text{out}}$  (see Section 3 in [25]). The noise at the output of the difference-field circuit in **Figure 4** is the sum of uncorrelated noises on both Hall plates.

$$v_{\text{diff},rms} = \sqrt{4k_b T (R_{\text{out}}(B_{\perp}) + R_{\text{out}}(-B_{\perp})) ENBW} \tag{4a}$$

$$i_{\text{diff},rms} = \sqrt{4k_b T (G_{\text{out}}(B_{\perp}) + G_{\text{out}}(-B_{\perp})) ENBW} \tag{4b}$$

The signal to noise ratio  $SNR^{(vm)}$  in voltage mode operation is defined as

$$SNR^{(vm)} = \frac{V_{\text{diff}}}{v_{\text{diff},rms}} = \frac{V_{\text{out}}(B_{\perp}) - V_{\text{out}}(-B_{\perp})}{\sqrt{4k_b T (R_{\text{out}}(B_{\perp}) + R_{\text{out}}(-B_{\perp})) ENBW}} \tag{5a}$$

The signal to noise ratio  $SNR^{(cm)}$  in current mode operation is defined as

$$SNR^{(cm)} = \frac{I_{\text{diff}}}{i_{\text{diff},rms}} = \frac{I_{\text{out}}(B_{\perp}) - I_{\text{out}}(-B_{\perp})}{\sqrt{4k_b T (G_{\text{out}}(B_{\perp}) + G_{\text{out}}(-B_{\perp})) ENBW}} \tag{5b}$$

Equation (5b) also gives the  $SNR$  in hybrid operating mode, which we call  $SNR^{(x)}$  (see (30)). In (5a, b) the  $SNR$  depends on the magnetic field  $B_{\perp}$ , on the Hall mobility  $\mu_{fp}$  on the absolute temperature  $T$ , on the effective noise bandwidth  $ENBW$  of the circuit, and on the power  $P_{\text{diff}}$  dissipated in the difference-field circuit. This is explained in (33) in [25]. Therefore, we define a dimension-less noise efficiency  $\eta$ , which is a normalized  $SNR$  independent of all these quantities.

$$\eta = \frac{SNR}{\mu_H B_{\perp}} \times \sqrt{\frac{4k_b T ENBW}{P_{\text{diff}}}} \tag{6}$$

with  $\mu_H B_{\perp} = \tan(\theta_H)$ ,  $\theta_H$  being the Hall angle. The noise efficiency is a sole function of the layout of the Hall plate (including the number of contacts), the patterns of the supply currents or voltages and the patterns of the weighing coefficients (with *patterns* we mean that a scaling by common factor is irrelevant).

Thus, it is a structural property of the Hall plate and the respective circuit of **Figures 1-4**, and it does not depend on any physical quantities such as Hall mobility or sheet resistance. For conventional Hall plates with four contacts being operated in voltage mode it is less or equal to  $\sqrt{2}/3 \cong 0.471$ , and for symmetric circular Hall plates with 40 contacts of identical size and same spacing it is 89% larger ( $=0.891$ ) [25].

In (6) we used the power  $P_{\text{diff}}$  of the difference-field circuit, which is larger than the power dissipated in the two Hall plates, because power is also dissipated in the current and voltage sources. The reason is the practical implementation of current and voltage sources with semiconductor devices (like MOS transistors) as shown in **Figure 5**. In fact these transistors are used as pass devices, which are connected between contacts of the Hall plate and terminals of the battery. Feedback circuits control their pass resistances in such a way that they deliver constant current or constant voltage. Thereby, the control loop of the feedback circuit simply dumps excess power in the pass devices. We call this case “lossy bias”.

The use of  $P_{\text{diff}}$  in (6) makes sense for integrated sensors, where the Hall plate and the circuit are on the same chip. Then, the total power of the circuit is relevant for heating up the chip. This is the case for commercial Hall sensors used in the industry. Conversely, there are other cases where one would only like to take account of the power dissipated in the Hall plate—not in the circuit. For instance, one may use a discrete Hall plate connected via long leads to an off-chip circuit being supplied from the mains supply. Then the dissipation of the bias circuit is less relevant, and one may use  $2P_{\text{Hall}}$  instead of  $P_{\text{diff}}$  in (6). We call this case “lossless bias”. This will lead to a slightly larger noise efficiency and to markedly different patterns of optimum supply currents, supply voltages, and coefficients, as it is elaborated in **Section 6**.

In a power optimized design of an integrated Hall sensor the battery voltage is chosen equal to the maximum voltage across a Hall plate plus some small headroom of around 150 mV for the pass device to operate it in the feedback loop. For the sake of simplicity we neglect this small headroom voltage.

$$P_{\text{diff}} = V_{\text{battery}} I_{\text{battery}} \tag{7a}$$

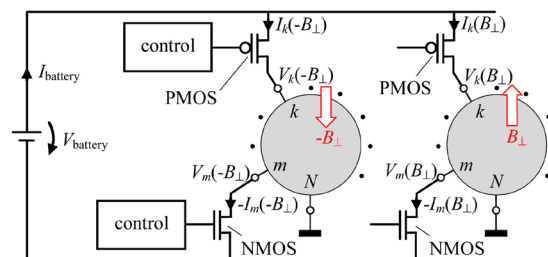


**Figure 5.** Definition of the total power of the difference-field circuit powered by a single battery. Two Hall plates are exposed to magnetic fields of the same magnitude and opposite polarity. The voltage and current sources are implemented as MOS transistors operated in feedback loops. We need to minimize the total power of the circuit, which is the sum of power in the Hall plates plus the power in the MOS transistors.

$$V_{\text{battery}} = \max \left\{ \max_{k \in [1, N-1]} V_k(B_{\perp}), \max_{k \in [1, N-1]} V_k(-B_{\perp}), 0 \right\} - \min \left\{ \min_{k \in [1, N-1]} V_k(B_{\perp}), \min_{k \in [1, N-1]} V_k(-B_{\perp}), 0 \right\} \quad (7b)$$

$$I_{\text{battery}} = \frac{1}{2} \left( \sum_{k=1}^{N-1} |I_k(B_{\perp})| + \left| \sum_{k=1}^{N-1} I_k(B_{\perp}) \right| + \sum_{k=1}^{N-1} |I_k(-B_{\perp})| + \left| \sum_{k=1}^{N-1} I_k(-B_{\perp}) \right| \right) \quad (7c)$$

In (7b) the zeros account for the potential of the grounded  $N$ -th contact.

### 3.2. Voltage-Mode Operation

From **Figure 1** and from (2a) the output voltage  $V_{\text{diff}}$  in the difference-field circuit is

$$V_{\text{diff}} = \mathbf{c}^T \cdot \mathbf{R}(B_{\perp}) \cdot \mathbf{I}_{\text{supply}} - \mathbf{c}^T \cdot \mathbf{R}(-B_{\perp}) \cdot \mathbf{I}_{\text{supply}} = \mathbf{c}^T \cdot (\mathbf{R} - \mathbf{R}^T) \cdot \mathbf{I}_{\text{supply}} \quad (8)$$

The vector  $\mathbf{c} = (c_1, c_2, \dots, c_{N-1})^T$  collects all weighing coefficients, and the definite resistance matrix  $\mathbf{R}$  relates currents  $\mathbf{I} = (I_1, I_2, \dots, I_{N-1})^T$  and voltages  $\mathbf{V} = (V_1, V_2, \dots, V_{N-1})^T$  at the contacts of the Hall plate according to  $\mathbf{V} = \mathbf{R} \cdot \mathbf{I}$ . The index “supply” in  $\mathbf{I}_{\text{supply}}$  reminds us that the currents do not change versus applied magnetic field, because they are impressed by the ideal current sources. The transpose of vector  $\mathbf{c}$  is  $\mathbf{c}^T$ , the transpose of matrix  $\mathbf{R}$  is  $\mathbf{R}^T$ . In the derivation of (8) we used the identity  $\mathbf{R}(-B_{\perp}) = \mathbf{R}^T(B_{\perp})$ , which is known as the principle of reverse magnetic field reciprocity (RMFR) [21] [22]. If we do not specify the magnetic field as an argument of a matrix, we mean positive magnetic field:  $\mathbf{R} = \mathbf{R}(B_{\perp})$ . Only for negative magnetic field we explicitly specify the negative magnetic field as an argument of the matrix:  $\mathbf{R}(-B_{\perp})$ .

For the calculation of thermal noise we need to know the output resistance of the circuit in **Figure 1**. This output resistance  $R_{\text{out}}$  takes into account the statistical correlations of noise voltages between all contacts in the multi-contact Hall plate, as it was explained in [25]. For the calculation of  $R_{\text{out}}$  we replace all current sources in **Figure 1** by opens, inject a current  $I_{\text{out}}$  into the secondary coils of all ideal transformers, and compute the resulting  $V_{\text{out}}$ . The ideal transformers couple the current into their primary coils  $\mathbf{I} = I_{\text{out}} \cdot \mathbf{c}$ . The Hall plate voltages respond to these currents with  $\mathbf{V} = \mathbf{R} \cdot \mathbf{I}$ . And finally, the ideal transformers couple these voltages to their secondary sides, where they are summed up  $V_{\text{out}} = \mathbf{c}^T \cdot \mathbf{V}$ . Combining these three equations gives the output resistance as a quadratic form

$$R_{\text{out}} = V_{\text{out}} / I_{\text{out}} = \mathbf{c}^T \cdot \mathbf{R} \cdot \mathbf{c} \quad (9)$$

Therefore the thermal noise voltage at the output of the difference-field circuit in **Figure 4** is

$$v_{\text{diff}, \text{rms}} = \sqrt{4k_b T \times ENBW} \mathbf{c}^T \cdot (\mathbf{R} + \mathbf{R}^T) \cdot \mathbf{c} \quad (10)$$

With (5a), the signal to noise ratio for voltage mode operation is

$$SNR^{(vm)} = \frac{\mathbf{c}^T \cdot (\mathbf{R} - \mathbf{R}^T) \cdot \mathbf{I}_{\text{supply}}}{\sqrt{4k_b T \times ENBW} \mathbf{c}^T \cdot (\mathbf{R} + \mathbf{R}^T) \cdot \mathbf{c}} \quad (11)$$

and with (6) the noise efficiency is

$$\eta^{(vm)} = \frac{1}{\tan(\theta_H) \sqrt{P_{\text{diff}}}} \times \frac{\mathbf{c}^T \cdot (\mathbf{R} - \mathbf{R}^T) \cdot \mathbf{I}_{\text{supply}}}{\sqrt{\mathbf{c}^T \cdot (\mathbf{R} + \mathbf{R}^T) \cdot \mathbf{c}}} \quad (12)$$

### 3.3. Current-Mode Operation

Turning now to the current mode operation in **Figure 2**.

$$I_{\text{out}} = \sum_{k=1}^N d_k I_k = \sum_{k=1}^{N-1} d_k I_k - d_N \sum_{k=1}^{N-1} I_k = \sum_{k=1}^{N-1} (d_k - d_N) I_k = (\mathbf{d} - d_N \mathbf{u})^T \cdot \mathbf{I} \quad (13)$$

In the derivation of (13) we used Kirchhoff's nodal current law to express the  $N$ -th current by the negative sum of all other currents. The coefficients  $d_k$  are collected in the vector  $\mathbf{d} = (d_1, d_2, \dots, d_{N-1})^T$ , and  $\mathbf{u} = (1, 1, \dots, 1)^T$  with  $N - 1$  components. With  $\mathbf{I} = \mathbf{G} \cdot \mathbf{V}$  and  $\mathbf{G} = \mathbf{R}^{-1}$ , it follows the output current  $I_{\text{diff}}$  in the difference-field circuit according to (2b)

$$I_{\text{diff}} = (\mathbf{d} - d_N \mathbf{u})^T \cdot (\mathbf{G} - \mathbf{G}^T) \cdot \mathbf{V}_{\text{supply}} \quad (14)$$

The index “supply” in  $\mathbf{V}_{\text{supply}}$  reminds us that the voltages do not change versus applied magnetic field, because they are impressed by ideal voltage sources. In (14) we used  $\mathbf{G}(-B_{\perp}) = \mathbf{G}^T$ , which is a direct consequence of the principle of RMFR [21] [22].

The noise current at the output of **Figure 2** is determined by the output conductance  $G_{\text{out}}$ . For its computation we replace all voltage sources by shorts. Then we apply a voltage  $V_{\text{out}}$  across the output terminal in **Figure 2** and compute the resulting current  $I_{\text{out}}$ . The  $N$ -th transformer lifts the potential of contact  $N$  by an amount  $d_N V_{\text{out}}$ . Therefore we have to use  $\mathbf{I} = \mathbf{G} \cdot (\mathbf{V} - V_{\text{out}} d_N \mathbf{u})$  instead of simply  $\mathbf{I} = \mathbf{G} \cdot \mathbf{V}$ . Inserting this into (13) and using  $\mathbf{V} = V_{\text{out}} \mathbf{d}$  gives

$$G_{\text{out}} = I_{\text{out}}/V_{\text{out}} = (\mathbf{d} - d_N \mathbf{u})^T \cdot \mathbf{G} \cdot (\mathbf{d} - d_N \mathbf{u}) \quad (15)$$

With (4b) the thermal noise current at the output of the difference-field circuit in **Figure 4** is given by

$$i_{\text{diff},rms} = \sqrt{4k_b T \times ENBW (\mathbf{d} - d_N \mathbf{u})^T \cdot (\mathbf{G} + \mathbf{G}^T) \cdot (\mathbf{d} - d_N \mathbf{u})} \quad (16)$$

With (14), (16), and (5b) we get the signal-to-noise ratio.

$$SNR^{(cm)} = \frac{(\mathbf{d} - d_N \mathbf{u})^T \cdot (\mathbf{G} - \mathbf{G}^T) \cdot \mathbf{V}_{\text{supply}}}{\sqrt{4k_b T \times ENBW (\mathbf{d} - d_N \mathbf{u})^T \cdot (\mathbf{G} + \mathbf{G}^T) \cdot (\mathbf{d} - d_N \mathbf{u})}} \quad (17)$$

In (17) we note that the  $N$ -th weighing coefficient  $d_N$  is subtracted from all other coefficients. Therefore  $d_N$  is superfluous: suppose we search for optimum coefficients with some arbitrary value for  $d_N$ , say 3. The resulting  $SNR$  is identical to the case, where  $d_N = 0$  and all other coefficients are reduced by 3. In other words, for arbitrary  $d_N$  the solution for  $\mathbf{d}$  is not unique, and therefore we define  $d_N = 0$ . Then we may also skip the  $N$ -th ideal transformer. This gives a formula for the  $SNR^{(cm)}$  in current mode operation, which is more similar to the  $SNR^{(vm)}$  in voltage mode operation.

$$SNR^{(cm)} = \frac{\mathbf{d}^T \cdot (\mathbf{G} - \mathbf{G}^T) \cdot \mathbf{V}_{supply}}{\sqrt{4k_b T \times ENBW} \sqrt{\mathbf{d}^T \cdot (\mathbf{G} + \mathbf{G}^T) \cdot \mathbf{d}}} \tag{18}$$

The noise efficiency is

$$\eta^{(cm)} = \frac{1}{\tan(\theta_H) \sqrt{P_{diff}}} \times \frac{\mathbf{d}^T \cdot (\mathbf{G} - \mathbf{G}^T) \cdot \mathbf{V}_{supply}}{\sqrt{\mathbf{d}^T \cdot (\mathbf{G} + \mathbf{G}^T) \cdot \mathbf{d}}} \tag{19}$$

### 3.4. The Hybrid Operating Mode

In the hybrid operating mode the Hall plate has  $N - 1$  contacts where either currents or voltages can be supplied. Thus, there exists a great number of  $2^{N-1}$  hybrid operating modes. We define an integer number  $x \in [0, 2^{N-1} - 1]$ , whose binary representation has  $N - 1$  bits. We define the hybrid operating mode number  $x$  as the one, where voltage sources are connected to contacts, which correspond to “1” in the binary representation of  $x$ . Thereby, the least significant bit (LSB) corresponds to contact 1, and the most significant bit (MSB) corresponds to contact  $N - 1$ .

*Example:* The 9-th hybrid operating mode of a Hall plate with 7 contacts has voltage sources connected to contacts 1 and 4, because  $x = 9 = 1 \times 2^3 + 1 \times 2^0$  with the binary representation  $x_{bin} = 001001$  (the LSB is at the right side of the bit pattern). Current sources are connected to the other contacts 2, 3, 5, and 6.

The zero-th hybrid operating mode ( $x = 0$ ) means that all contacts are supplied by current sources. This is the conventional voltage mode operation. Conversely, the hybrid operating mode  $2^{N-1} - 1$  means that all contacts are supplied by voltage sources, which is the conventional current mode operation.

Next we define a vector  $\mathbf{A}^{(x)}$  of voltages and currents.

$$\mathbf{A}^{(x)} = \text{diag}(x_{bin}) \cdot \mathbf{V} + \text{diag}(\bar{x}_{bin}) \cdot \mathbf{I} = \mathbf{X} \cdot \mathbf{V} + \bar{\mathbf{X}} \cdot \mathbf{I} \tag{20}$$

In (20),  $\mathbf{X} = \text{diag}(x_{bin})$  is an  $(N - 1) \times (N - 1)$  diagonal matrix, which has the bits of the binary representation of  $x$  on its main diagonal, whereby the LSB is at the crossing of column 1 and row 1 and the MSB is at the crossing of column  $N - 1$  and row  $N - 1$ .  $\bar{\mathbf{X}}$  is singular, except for current mode operation  $x = 2^{N-1} - 1$ . Moreover,  $\bar{x}_{bin}$  is obtained from  $x_{bin}$  by swapping all ones and zeros. It holds

$$x + \bar{x} = 2^{N-1} - 1 \tag{21a}$$

$$\mathbf{X} + \bar{\mathbf{X}} = \mathbf{1} \tag{21b}$$

$$\mathbf{X} \cdot \bar{\mathbf{X}} = \bar{\mathbf{X}} \cdot \mathbf{X} = \mathbf{0} \tag{21c}$$

$$\mathbf{X} \cdot \mathbf{X} = \mathbf{X} \quad \text{and} \quad \bar{\mathbf{X}} \cdot \bar{\mathbf{X}} = \bar{\mathbf{X}} \tag{21d}$$

$$(\mathbf{X} - \bar{\mathbf{X}})^{-1} = \mathbf{X} - \bar{\mathbf{X}} \tag{21e}$$

where  $\mathbf{1}$  is the unit matrix and  $\mathbf{0}$  is the zero matrix. With (21a-d) we can retrieve voltage and current vectors from (20).

$$V = X \cdot A^{(x)} + \bar{X} \cdot A^{(\bar{x})} \quad (22a)$$

$$I = \bar{X} \cdot A^{(x)} + X \cdot A^{(\bar{x})} \quad (22b)$$

Next we define the hybrid matrix  $H^{(x)}$  describing the hybrid operating mode with the number  $x$  like this

$$A^{(\bar{x})} = H^{(x)} \cdot A^{(x)} \quad (23a)$$

If we insert all supply currents and voltages into  $A^{(x)}$ , (23a) gives us  $A^{(\bar{x})}$ , which is all output voltages and currents of the Hall plate. The two vectors  $A^{(x)}$  and  $A^{(\bar{x})}$  are complementary: if the  $k$ -th element of  $A^{(x)}$  is a current, the  $k$ -th element of  $A^{(\bar{x})}$  is a voltage, and vice versa. Therefore some elements of  $A^{(x)}$  have the dimension of a voltage and others have the dimension of a current. Consequently, some entries of  $H^{(x)}$  have the dimension 1, while others have the dimension of a resistance or a conductance. The power dissipated in a Hall plate is

$$P_{Hall} = \left(A^{(x)}\right)^T \cdot A^{(\bar{x})} = \left(A^{(x)}\right)^T \cdot H^{(x)} \cdot A^{(x)} > 0 \quad (23b)$$

Since the Hall plate is passive and dissipative, this power is positive for all  $A^{(x)} \neq \mathbf{0}$ . Therefore,  $H^{(x)}$  is a positive definite matrix. Consequently, it is non-singular. From (23a) it follows

$$H^{(\bar{x})} = \left(H^{(x)}\right)^{-1} \quad (24)$$

Yet,  $H^{(x)}$  is *not* symmetric (see (36b), (58b)). Next we take (23a) and replace the  $A$ -vectors with the help of (20). Then we replace  $V$  by  $R \cdot I$ . This gives

$$\left(\bar{X} \cdot R + X\right) \cdot I = H^{(x)} \cdot \left(X \cdot R + \bar{X}\right) \cdot I \quad (25a)$$

(25a) must hold for arbitrary current vectors  $I$ . Therefore it follows

$$\bar{X} \cdot R + X = H^{(x)} \cdot \left(X \cdot R + \bar{X}\right) \quad (25b)$$

In **Appendix B** we prove that  $X \cdot R + \bar{X}$  is not singular. Thus, we can express the hybrid matrix in terms of the resistance matrix.

$$H^{(x)} = \left(\bar{X} \cdot R + X\right) \cdot \left(X \cdot R + \bar{X}\right)^{-1} \quad (26a)$$

Two special cases follow from (26a)

$$H^{(0)} = R \quad \text{and} \quad H^{(2^{N-1}-1)} = G, \quad (26b)$$

and they are in accordance with (24). The hybrid matrix at negative magnetic field is

$$H^{(x)}(-B_{\perp}) = \left(\bar{X} \cdot R^T + X\right) \cdot \left(X \cdot R^T + \bar{X}\right)^{-1} \quad (26c)$$

where we used the principle of RMFR  $R(-B_{\perp}) = \left(R(B_{\perp})\right)^T$  [21] [22]. In general, hybrid matrices are *not* reverse magnetic field reciprocal, *i.e.*,

$H^{(x)}(-B_{\perp}) \neq \left(H^{(x)}(B_{\perp})\right)^T$ , except for  $x = 0$  and  $x = 2^{N-1} - 1$ . Instead, the following relations between matrices at opposite magnetic field polarity hold (see **Appendix C**).

$$\mathbf{H}^{(x)}(-B_{\perp}) = (\mathbf{X} - \bar{\mathbf{X}}) \cdot \left( \mathbf{H}^{(x)}(B_{\perp}) \right)^{\top} \cdot (\mathbf{X} - \bar{\mathbf{X}}) \tag{27a}$$

$$\mathbf{H}^{(x)}(-B_{\perp}) \cdot (\mathbf{X} - \bar{\mathbf{X}}) = \left( \mathbf{H}^{(x)}(B_{\perp}) \cdot (\mathbf{X} - \bar{\mathbf{X}}) \right)^{\top} \tag{27b}$$

(27b) follows from (27a) with (C2). (27b) means that  $\mathbf{H}^{(x)} \cdot (\mathbf{X} - \bar{\mathbf{X}})$  is reverse magnetic field reciprocal. We call this the principle of hybrid reverse magnetic field reciprocity (HRMFR). The diagonal matrix  $(\mathbf{X} - \bar{\mathbf{X}})$  has only  $\pm 1$  on its main diagonal. Therefore (27b) simply states

$$H_{m,k}^{(x)}(-B_{\perp}) = \pm H_{k,m}^{(x)}(B_{\perp}) \quad \forall k \neq m \tag{27c}$$

$$H_{k,k}^{(x)}(-B_{\perp}) = H_{k,k}^{(x)}(B_{\perp}) > 0 \quad \forall k \tag{27d}$$

The positive sign in (27c) holds if the  $k$ -th and the  $m$ -th bit of  $x_{\text{bin}}$  are identical, which means that  $k$ -th and the  $m$ -th element in  $\mathbf{A}^{(x)}$  are either both voltages, or they are both currents. This corresponds to the dimension of  $H_{m,k}^{(x)}$  and  $H_{k,m}^{(x)}$  being 1. Then, the symmetry of the elements  $H_{m,k}^{(x)}$  and  $H_{k,m}^{(x)}$  is analogous to the symmetry of the  $\mathbf{R}$  and  $\mathbf{G}$  matrices according to the principle of RMFR. Accordingly, the negative sign in (27c) holds if the dimension of  $H_{m,k}^{(x)}$  and  $H_{k,m}^{(x)}$  is a resistance or a conductance.

(27d) also states that all elements on the main diagonal of all hybrid matrices are positive. This is a general property of real positive definite matrices. It also follows from the definition (23a), which says that  $H_{k,k}^{(x)}$  is the ratio of current over voltage (or its reciprocal) at the  $k$ -th contact, whereby all other contacts of the Hall plate are tied to ground or left open. Therefore power enters the Hall plate only through the  $k$ -th contact. Since the Hall plate is a passive and dissipative device, it can only absorb power, which means that the product of current and voltage at the  $k$ -th contact is positive. Consequently, also the ratio of both is positive.

With (2b) the output signal in the difference-field circuit of **Figure 4** is

$$I_{\text{diff}} = \mathbf{h}^{\top} \cdot \left( \mathbf{H}^{(x)}(B_{\perp}) - \mathbf{H}^{(x)}(-B_{\perp}) \right) \cdot \mathbf{A}_{\text{supply}}^{(x)} \tag{28}$$

where  $\mathbf{A}_{\text{supply}}^{(x)}$  is the  $\mathbf{A}$ -vector with all supply voltages and supply currents according to the binary bit pattern of  $x$ .

Next we compute the output conductance  $G_{\text{out}}$ . To this end we replace all voltage sources by shorts and all current sources by opens in **Figure 3**. Then we replace the ampere-meter by a voltage source that applies  $V_{\text{out}}$  to the secondary sides of the ideal transformers and gyrators. They couple  $V_{\text{out}}$  to their primary sides, which gives  $\mathbf{A}^{(x)} = -V_{\text{out}} \mathbf{h}$ . The Hall plate responds with  $\mathbf{H}^{(x)} \cdot \mathbf{A}^{(x)}$ . The transformers and gyrators couple that again to their secondary sides, where the parallel connection sums up these contributions to the current  $I_{\text{out}}$ . This gives

$$G_{\text{out}} = I_{\text{out}} / V_{\text{out}} = \mathbf{h}^{\top} \cdot \mathbf{H}^{(x)} \cdot \mathbf{h} = \sum_{m < k} h_m h_k \left( H_{m,k}^{(x)} + H_{k,m}^{(x)} \right) + \sum_m h_m^2 H_{m,m}^{(x)} \tag{29}$$

If we toggle the polarity of the magnetic field in (29) the second sum on the RHS remains identical due to (27d). Yet, only those terms in the first sum on the

RHS remain identical, where  $k$ -th and the  $m$ -th bit of  $x_{\text{bin}}$  are identical—all other terms change their sign. Hence, in contrast to (9) and (15) the output conductance in (29) depends on the polarity of the magnetic field, except for  $x = 0$  and  $x = 2^{N-1} - 1$ .

For the SNR of the difference-field circuit in Figure 4 in hybrid operating mode we get from (5b) with (27a)

$$SNR^{(x)} = \frac{\mathbf{h}^T \cdot \left[ \mathbf{H}^{(x)} - (\mathbf{X} - \bar{\mathbf{X}}) \cdot (\mathbf{H}^{(x)})^T \cdot (\mathbf{X} - \bar{\mathbf{X}}) \right] \cdot \mathbf{A}_{\text{supply}}^{(x)}}{\sqrt{4k_b T \times ENBW} \sqrt{\mathbf{h}^T \cdot \left[ \mathbf{H}^{(x)} + (\mathbf{X} - \bar{\mathbf{X}}) \cdot (\mathbf{H}^{(x)})^T \cdot (\mathbf{X} - \bar{\mathbf{X}}) \right] \cdot \mathbf{h}}} \quad (30)$$

With (6) we get the noise efficiency

$$\eta^{(x)} = \frac{1}{\tan(\theta_H) \sqrt{P_{\text{diff}}}} \times \frac{\mathbf{h}^T \cdot \left[ \mathbf{H}^{(x)} - (\mathbf{X} - \bar{\mathbf{X}}) \cdot (\mathbf{H}^{(x)})^T \cdot (\mathbf{X} - \bar{\mathbf{X}}) \right] \cdot \mathbf{A}_{\text{supply}}^{(x)}}{\sqrt{\mathbf{h}^T \cdot \left[ \mathbf{H}^{(x)} + (\mathbf{X} - \bar{\mathbf{X}}) \cdot (\mathbf{H}^{(x)})^T \cdot (\mathbf{X} - \bar{\mathbf{X}}) \right] \cdot \mathbf{h}}} \quad (31)$$

#### 4. The SNR at Weak Magnetic Field

At weak magnetic field we assume that the power in the Hall plate and the thermal noise are equal to the ones at zero magnetic field. This assumption is supported by the fact that power and noise are defined by the even parts of the resistance matrix, which comprise only even order powers of the magnetic field. Hence, in a linear (first order) approximation, they become independent of the magnetic field. We use Taylor series expansions for the resistance matrix and the hybrid matrices into powers of the magnetic field, and we discard powers of higher than first order.

$$\mathbf{H}^{(x)} = \mathbf{H}_0^{(x)} + \mathbf{H}_1^{(x)} + O^2(B_{\perp}) \quad \text{and} \quad \mathbf{R} = \mathbf{R}_0 + \mathbf{R}_1 + O^2(B_{\perp}) \quad (32)$$

$\mathbf{R}_0$  and  $\mathbf{H}_0^{(x)}$  are the resistance matrix and the hybrid matrix at zero magnetic field, respectively.  $\mathbf{R}_1$  and  $\mathbf{H}_1^{(x)}$  are the small changes of both matrices due to small magnetic field. Both are linearly proportional to the magnetic field. Therefore, the following reverse magnetic field symmetries hold.

$$\mathbf{H}_1^{(x)}(-B_{\perp}) = -\mathbf{H}_1^{(x)}(B_{\perp}) \quad \text{and} \quad \mathbf{R}_1(-B_{\perp}) = -\mathbf{R}_1(B_{\perp}) \quad (33)$$

In the voltage mode ( $x = 0$ ) we call the currents  $\mathbf{I}_{\text{supply}}^{(0)}$  and at zero magnetic field they lead to the voltages  $\mathbf{V}^{(0)} = \mathbf{R}_0 \mathbf{I}_{\text{supply}}^{(0)}$ . In all other hybrid modes ( $x > 0$ ) we keep the currents  $\mathbf{I}_{\text{supply}}^{(0)}$  at all contacts with current sources, and we apply voltages  $\mathbf{V}^{(0)}$  at all contacts with voltage sources. This procedure ensures that we keep the powers at all contacts constant, and therefore also the powers in the MOS-transistors in Figure 5 remain the same, and finally the total power of the difference-field circuit remains also constant in all hybrid operating modes. This is a necessary requirement if we want to compare SNR in different hybrid operating modes. With (20) we get the supply vector in hybrid operating mode number  $x$

$$A_{\text{supply}}^{(x)} = X \cdot V^{(0)} + \bar{X} \cdot I_{\text{supply}}^{(0)} = (X \cdot R_0 + \bar{X}) \cdot I_{\text{supply}}^{(0)} \tag{34}$$

Inserting (32) and (33) into (28) gives

$$I_{\text{diff}} = 2\mathbf{h}^T \cdot \mathbf{H}_1^{(x)} \cdot A_{\text{supply}}^{(x)} \tag{35}$$

From (27a) it follows at zero magnetic field

$$\mathbf{H}_0^{(x)} = (X - \bar{X}) \cdot (\mathbf{H}_0^{(x)})^T \cdot (X - \bar{X}) \tag{36a}$$

$$(\mathbf{H}_0^{(x)})^T = (X - \bar{X}) \cdot \mathbf{H}_0^{(x)} \cdot (X - \bar{X}) \tag{36b}$$

We insert (34), (35), and (36a) in (31) and get

$$\eta_0^{(x)} = \frac{\sqrt{2}}{\tan(\theta_H) \sqrt{P_{\text{diff}}}} \times \frac{\mathbf{h}^T \cdot \mathbf{H}_1^{(x)} \cdot (X \cdot R_0 + \bar{X}) \cdot I_{\text{supply}}^{(0)}}{\sqrt{\mathbf{h}^T \cdot \mathbf{H}_0^{(x)} \cdot \mathbf{h}}} \tag{37}$$

The index “0” in  $\eta_0^{(x)}$  denotes the noise efficiency in the limit of weak magnetic field. We insert the Taylor series ansatz (32) for the hybrid and the resistance matrices into (26a). This gives

$$\mathbf{H}_0^{(x)} \cdot (X \cdot R_0 + \bar{X}) = \bar{X} \cdot R_0 + X \tag{38a}$$

$$\mathbf{H}_1^{(x)} \cdot (X \cdot R_0 + \bar{X}) = (\bar{X} - \mathbf{H}_0^{(x)} \cdot X) \cdot R_1 \tag{38b}$$

Inserting (38b) into (37) gives

$$\eta_0^{(x)} = \frac{\sqrt{2}}{\tan(\theta_H) \sqrt{P_{\text{diff}}}} \times \frac{\mathbf{h}^T \cdot (\bar{X} - \mathbf{H}_0^{(x)} \cdot X) \cdot R_1 \cdot I_{\text{supply}}^{(0)}}{\sqrt{\mathbf{h}^T \cdot \mathbf{H}_0^{(x)} \cdot \mathbf{h}}} \tag{39}$$

Our final goal is to maximize the noise efficiency  $\eta_0^{(x)}$  by choosing adequate coefficients  $\mathbf{h}$ . Thereby, we should not be surprised if  $\mathbf{h}$  depends on  $x$ . Until now, the coefficients  $\mathbf{h}$  are still unknown. A comparison of (39) with (12) suggests replacing the old coefficients  $\mathbf{h}$  by new coefficients  $\mathbf{c}$  according to

$$\mathbf{c}^T = \mathbf{h}^T \cdot (\bar{X} - \mathbf{H}_0^{(x)} \cdot X) \tag{40a}$$

From (40a) we get

$$\mathbf{h}^T = \mathbf{c}^T \cdot (\bar{X} - \mathbf{H}_0^{(x)} \cdot X)^{-1} \tag{40b}$$

$$\mathbf{h} = \left( \bar{X} - X \cdot (\mathbf{H}_0^{(x)})^T \right)^{-1} \cdot \mathbf{c} \tag{40c}$$

Inserting (40b, c) into (39) gives

$$\eta_0^{(x)} = \frac{\sqrt{2}}{\tan(\theta_H) \sqrt{P_{\text{diff}}}} \times \frac{\mathbf{c}^T \cdot R_1 \cdot I_{\text{supply}}^{(0)}}{\sqrt{\mathbf{c}^T \cdot (\bar{X} - \mathbf{H}_0^{(x)} \cdot X)^{-1} \cdot \mathbf{H}_0^{(x)} \cdot (\bar{X} - X \cdot (\mathbf{H}_0^{(x)})^T)^{-1} \cdot \mathbf{c}}} \tag{41}$$

With

$$\begin{aligned} (\bar{X} - \mathbf{H}_0^{(x)} \cdot X)^{-1} \cdot \mathbf{H}_0^{(x)} &= \left[ (\mathbf{H}_0^{(x)})^{-1} \cdot (\bar{X} - \mathbf{H}_0^{(x)} \cdot X) \right]^{-1} \\ &= \left( (\mathbf{H}_0^{(x)})^{-1} \cdot \bar{X} - X \right)^{-1} \end{aligned} \tag{42}$$

we can rewrite (41) like this

$$\eta_0^{(x)} = \frac{\sqrt{2}}{\sqrt{P_{\text{diff}}}} \times \frac{\mathbf{c}^T \cdot (\mathbf{R}_1 / \tan \theta_H) \cdot \mathbf{I}_{\text{supply}}^{(0)}}{\sqrt{\mathbf{c}^T \cdot \mathbf{Q} \cdot \mathbf{c}}} \quad (43a)$$

$$\mathbf{Q} = \left[ \left( \bar{\mathbf{X}} - \mathbf{X} \cdot (\mathbf{H}_0^{(x)})^T \right) \cdot \left( (\mathbf{H}_0^{(x)})^{-1} \cdot \bar{\mathbf{X}} - \mathbf{X} \right) \right]^{-1} \quad (43b)$$

In (43a) the quadratic form  $\mathbf{c}^T \cdot \mathbf{Q} \cdot \mathbf{c}$  discards the skew-symmetric part of  $\mathbf{Q}$ .

$$\mathbf{c}^T \cdot \mathbf{Q} \cdot \mathbf{c} = \mathbf{c}^T \cdot \left( \frac{\mathbf{Q} + \mathbf{Q}^T}{2} + \frac{\mathbf{Q} - \mathbf{Q}^T}{2} \right) \cdot \mathbf{c} = \mathbf{c}^T \cdot \frac{\mathbf{Q} + \mathbf{Q}^T}{2} \cdot \mathbf{c} \quad (44)$$

From its definition (43b),  $\mathbf{Q}$  is a function of  $x$ . If we replace  $x$  by  $\bar{x}$  we get  $\bar{\mathbf{Q}}$  from  $\mathbf{Q}$ . It holds

$$\begin{aligned} \bar{\mathbf{Q}} &= \left[ \left( \mathbf{X} - \bar{\mathbf{X}} \cdot (\mathbf{H}_0^{(\bar{x})})^T \right) \cdot \left( (\mathbf{H}_0^{(\bar{x})})^{-1} \cdot \mathbf{X} - \bar{\mathbf{X}} \right) \right]^{-1} \\ &= \left[ \left( \mathbf{X} - \bar{\mathbf{X}} \cdot \left( (\mathbf{H}_0^{(x)})^{-1} \right)^T \right) \cdot \left( \mathbf{H}_0^{(x)} \cdot \mathbf{X} - \bar{\mathbf{X}} \right) \right]^{-1} \\ &= \left\{ \left[ \left( \mathbf{X} \cdot (\mathbf{H}_0^{(x)})^T - \bar{\mathbf{X}} \right) \cdot \left( \mathbf{X} - (\mathbf{H}_0^{(x)})^{-1} \cdot \bar{\mathbf{X}} \right) \right]^{-1} \right\}^T = \mathbf{Q}^T \end{aligned} \quad (45)$$

With (43a) we see that for identical coefficient vectors  $\mathbf{c}$  we get identical noise efficiencies in complementary hybrid operating modes  $x$  and  $\bar{x}$ .

$$\eta_0^{(x)} = \eta_0^{(\bar{x})} \quad (46)$$

In particular, (46) means for  $x = 0$ ,  $\bar{x} = 2^{N-1} - 1$  that the noise efficiencies in voltage and current operating modes are identical. However, we can show an even more general equivalence: *the noise efficiencies of all hybrid operating modes are identical for identical coefficients  $\mathbf{c}$* . This follows from the identity

$$\mathbf{Q} = \mathbf{R}_0 \cdot \bar{\mathbf{X}} + \mathbf{X} \cdot \mathbf{R}_0 \quad (47)$$

which is proven in **Appendix D**. Inserting (47) into (44) gives

$$\mathbf{c}^T \cdot \frac{\mathbf{Q} + \mathbf{Q}^T}{2} \cdot \mathbf{c} = \mathbf{c}^T \cdot \frac{\mathbf{R}_0 \cdot \bar{\mathbf{X}} + \mathbf{X} \cdot \mathbf{R}_0 + (\mathbf{R}_0 \cdot \bar{\mathbf{X}} + \mathbf{X} \cdot \mathbf{R}_0)^T}{2} \cdot \mathbf{c} = \mathbf{c}^T \cdot \mathbf{R}_0 \cdot \mathbf{c} \quad (48)$$

and finally this leads to the noise efficiency

$$\eta_0^{(x)} = \sqrt{\frac{2}{P_{\text{diff}}}} \frac{\mathbf{c}^T \cdot (\mathbf{R}_1 / \tan(\theta_H)) \cdot \mathbf{I}_{\text{supply}}^{(0)}}{\sqrt{\mathbf{c}^T \cdot \mathbf{R}_0 \cdot \mathbf{c}}} = \eta_0^{(0)} \quad (49)$$

which is independent of  $x$ , and therefore we can simply call it  $\eta_0$ . (49) says that for an arbitrary set of supply currents  $\mathbf{I}_{\text{supply}}^{(0)}$  in voltage mode operation and for an arbitrary set of coefficients  $\mathbf{c}$ , all hybrid operating modes have the same noise efficiency. There are only three necessary requirements: 1) the magnetic field is weak, 2) the coefficients  $\mathbf{c}$  are the same for all hybrid operating modes, and 3) the current and voltage supplies in the hybrid operating modes are given by (34).

Thereby, the gyrator trans-resistances and the transformer turns ratios are given by  $\mathbf{h}$  according to (40c). Moreover, the powers at all contacts, the total output signal, the output resistance, the power in the Hall plate, the power in the MOS-transistors, the total power of the difference-field circuit, and the  $SNR$  are identical in all hybrid operating modes.

In (40a) we introduced  $\mathbf{c}$  simply as a new vector. This led us to (49), which is identical to (12) in the limit of weak magnetic field. Thereby,  $\mathbf{R}_0$ ,  $\mathbf{R}_1$ , and  $\mathbf{I}_{\text{supply}}^{(0)}$  are arbitrary. Therefore,  $\mathbf{c}$  in (40a) is identical to the coefficient vector  $\mathbf{c}$  in (12) and in **Figure 1**.

Equation (49) must also hold for  $x = 2^{N-1} - 1$ . Comparison with (19) gives the identity

$$\mathbf{d} = \mathbf{R}_0 \cdot \mathbf{c} \tag{50a}$$

If we take the transpose of (40a) and insert (36b) and (26a) at zero magnetic field we get a simple relation between the coefficients  $\mathbf{c}, \mathbf{d}, \mathbf{h}$ .

$$\mathbf{h} = (\bar{\mathbf{X}} - \mathbf{X} \cdot \mathbf{R}_0) \cdot \mathbf{c} = \bar{\mathbf{X}} \cdot \mathbf{c} - \mathbf{X} \cdot \mathbf{d} \tag{50b}$$

With respect to maximum  $SNR$ , (49) shows that *optimum*  $\mathbf{c}$  and *optimum*  $\mathbf{I}_{\text{supply}}^{(0)}$  do not depend on  $x$ , *i.e.*, they are constant for all hybrid operating modes. In words, for all hybrid operating modes we can find optimum supply vectors  $\mathbf{A}_{\text{supply}}^{(x)}$  from (34) and optimum coefficients  $\mathbf{h}$  from (50b), which give the same maximum noise efficiency. With regard to noise efficiency, no hybrid operating mode is superior.

For the optimization of the noise efficiency in (49) we can use steps 1 and 2 of **Section 6**. Since  $\mathbf{R}_0$  is positive definite, it has a unique positive definite square-root  $\mathbf{R}_0^{1/2}$ . *Step 1:* We define a new vector

$$\mathbf{v}_2 = \mathbf{R}_0^{1/2} \cdot \mathbf{c} \tag{51}$$

Inserting (51) into (49) gives

$$\eta_0 = \sqrt{\frac{2}{P_{\text{diff}}}} \frac{\mathbf{v}_2^T \cdot \mathbf{R}_0^{-1/2} \cdot (\mathbf{R}_1 / \tan(\theta_H)) \cdot \mathbf{I}_{\text{supply}}^{(0)}}{\sqrt{\mathbf{v}_2^T \cdot \mathbf{v}_2}} \tag{52}$$

*Step 2:* The inequality of Cauchy-Schwartz gives

$$\mathbf{v}_2^T \cdot \mathbf{R}_0^{-1/2} \cdot \mathbf{R}_1 \cdot \mathbf{I}_{\text{supply}}^{(0)} \leq \sqrt{\mathbf{v}_2^T \cdot \mathbf{v}_2} \times \sqrt{(\mathbf{R}_0^{-1/2} \cdot \mathbf{R}_1 \cdot \mathbf{I}_{\text{supply}}^{(0)})^T \cdot \mathbf{R}_0^{-1/2} \cdot \mathbf{R}_1 \cdot \mathbf{I}_{\text{supply}}^{(0)}} \tag{53}$$

For maximum noise efficiency, equality holds in (53). Then  $\mathbf{v}_2$  and  $\mathbf{R}_0^{-1/2} \cdot \mathbf{R}_1 \cdot \mathbf{I}_{\text{supply}}^{(0)}$  are parallel (colinear), and the coefficients follow from the currents

$$\mathbf{c}_{\text{opt}} = s \mathbf{R}_0^{-1} \cdot \mathbf{R}_1 \cdot \mathbf{I}_{\text{supply, opt}}^{(0)} \tag{54}$$

with an arbitrary real number  $s \neq 0$ . Inserting (53) into (52) gives

$$\eta_{0, \text{opt}}^2 = \frac{2}{P_{\text{diff}}} \left( \mathbf{I}_{\text{supply, opt}}^{(0)} \right)^T \cdot \frac{\mathbf{R}_1^T}{\tan(\theta_H)} \cdot \mathbf{G}_0 \cdot \frac{\mathbf{R}_1}{\tan(\theta_H)} \cdot \mathbf{I}_{\text{supply, opt}}^{(0)} \tag{55}$$

In mathematics, (55) is known as a “fractional program” optimization prob-

lem. It is more general than (63c) due to the complicated form of  $P_{\text{diff}}$  (see (7a-c)). We have not found an analytical solution, but numerical optimization is feasible.

## 5. Numerical Examples

For asymmetric Hall plates several near-optimal solutions exist. It can be challenging for a numerical algorithm to find the overall maximum noise efficiency, as the following example shows.

Assume a non-optimal circular Hall plate with four asymmetric contacts subtending the intervals of azimuth angles  $[0^\circ, 45^\circ]$ ,  $[97^\circ, 195^\circ]$ ,  $[217^\circ, 271^\circ]$ , and  $[282^\circ, 311^\circ]$ . Hence, the sizes of the contacts are  $45^\circ$ ,  $98^\circ$ ,  $54^\circ$ ,  $29^\circ$  and their spacings are  $52^\circ$ ,  $22^\circ$ ,  $11^\circ$ ,  $49^\circ$ . The last contact is grounded. At weak magnetic field and for a sheet resistance of  $1 \Omega$  we can decompose the resistance matrix into the following even and odd parts.

$$\mathbf{R}_0 = \begin{pmatrix} 1.285810 & 0.702521 & 0.455935 \\ 0.702521 & 1.194200 & 0.603005 \\ 0.455935 & 0.603005 & 0.885051 \end{pmatrix} \quad (56a)$$

$$\lim_{\theta_H \rightarrow 0} \frac{\mathbf{R}_1}{\tan(\theta_H)} = \begin{pmatrix} 0 & 0.309820 & 0.280980 \\ -0.309820 & 0 & 0.233576 \\ -0.280980 & -0.233576 & 0 \end{pmatrix} \quad (56b)$$

whereby we used the method of [14]. We use (55) and (7a-c) to search for optimum supply currents and coefficients. In case #1 we start the numerical search with the current vector  $\mathbf{I}_{\text{supply}}^{(0)} = (0, 1, 0)^\top$ . Then we get  $\eta_0 = 0.4461510$  with the same current and with the coefficient vector

$\mathbf{c} = (0.654388, -0.00314656, -0.756152)^\top$ . This is the traditional voltage operating mode, where current enters in contact 2 and flows to contact 4, while voltage is tapped mainly at contacts 1 and 3 and a small portion of contact 2 is also added ( $c_2$  is small). In case #2 we use a different starting point  $\mathbf{I}_{\text{supply}}^{(0)} = (0, 1, 1)^\top$ . Then the optimization procedure returns a slightly smaller noise efficiency  $\eta_0 = 0.4456471$  with supply currents  $\mathbf{I}_{\text{supply}}^{(0)} = (-0.7968, 0.8094, 1)^\top$  and coefficients  $\mathbf{c} = (0.493397, 0.615044, -0.615044)^\top$ . This corresponds to a different voltage operating mode, where current flows into contacts 2 and 3 and out of contacts 1 and 4. Alternatively, we can connect contacts 2 and 3 to supply voltage and contacts 1 and 4 to ground  $\mathbf{V} = \mathbf{R}_0 \cdot \mathbf{I}_{\text{supply}}^{(0)} = (0, 1.00984, 1.00984)^\top$ , which means current operating mode. Regardless of voltage or current operating mode, case #2 does not give the global maximum noise efficiency. The tiny difference in noise performance for cases #1 and #2 seems to originate from the asymmetry of the Hall plate—for symmetrical Hall plates the noise efficiency in both cases would be identical.

In case #1 it might be surprising for experienced engineers that for optimum noise we got  $c_2 \neq 0$ . The four contacts Hall plate is supplied by a single current source at contact 2, and therefore the voltage at this contact does not respond to

the magnetic field in the weak field approximation ( $R_{22}$  is an even function of  $B_{\perp}$ , it has no linear term  $\propto B_{\perp}$ ). Thus, our theory says that even though contact 2 does not provide a Hall voltage, we should tap it and add a small contribution  $c_2 V_2$  to the total output signal, because this reduces the output resistance  $R_{out}$  by 19.5 ppm and therefore the thermal noise in the output signal. Yet, the benefit is really tiny and probably not worth while in practice.

We have done a number of numerical optimizations for Hall plates with three up to 40 contacts, which we do not report here in detail. They all showed that the components of the optimized current vectors in voltage operating mode have the following specific values: at some contacts they vanish, while at other contacts they have values which make the voltages at these contacts equal to 0 V or  $V_{supply}$  at zero magnetic field. This is consistent with our previous example. In such cases it holds  $P_{diff} = 2P_{Hall}$ , because there is no voltage drop over the pass devices (no voltage drops over the drain-source channels of the MOS transistors in **Figure 5**). This also goes along with an engineer’s intuition, because all available power of the battery is invested in the two Hall plates and none is wasted in the MOS-transistors. Yet, we have no stringent proof for this. Nevertheless, for practical purposes it seems to be a good strategy to compute the noise efficiency of all these cases, because chances are high that the global optimum is amongst them.

To this end, we assign a contact configuration number 0, 1, or 2 to each contact, which is grounded, or connected to  $V_{supply} = 1$  V, or left open, respectively. At least one contact must be connected to  $V_{supply}$ —otherwise the Hall plate is powered down. There are  $3^{N-1} - 2^{N-1}$  possible configurations (there are  $N - 1$  free contacts; at each contact we have three possibilities; but we have to subtract all possibilities where not a single contact is connected to the supply voltage). This means a total of five possible configurations for a three-contacts Hall plate, 19 configurations for a four-contacts Hall plate, 2059 configurations for a Hall plate with eight contacts, and  $\approx 4 \times 10^{18}$  configurations for a Hall plate with 40 contacts. In each configuration the supply vector  $A_{supply,opt}^{(x)}$  has entries equal to 1 at the positions corresponding to all contacts which are connected to the supply voltage, all other entries are equal to zero. With (22b) and (23a) we get the current vector

$$I_{supply,opt}^{(0)} = (\bar{X} + X \cdot H_0^{(x)}) \cdot A_{supply,opt}^{(x)} \tag{57}$$

Moreover, the following two relations hold

$$R^T = R(-B_{\perp}) \Rightarrow R_0^T + R_1^T = R_0 - R_1 \Rightarrow R_1^T = -R_1 \tag{58a}$$

$$\begin{aligned} H^{(x)}(-B_{\perp}) &= H_0^{(x)} - H_1^{(x)} = (X - \bar{X}) \cdot (H_0^{(x)} + H_1^{(x)})^T \cdot (X - \bar{X}) \\ &\Rightarrow (H_1^{(x)})^T = -(X - \bar{X}) \cdot H_1^{(x)} \cdot (X - \bar{X}) \end{aligned} \tag{58b}$$

In words,  $R_1$  and  $H_1^{(x)} \cdot (X - \bar{X})$  are skew-symmetric. In (58a) we used the principle of RMFR, and in (58b) we used (27a) together with (32). Inserting (57), (58a), and (58b) into (31) and using  $P_{diff} = 2P_{Hall}$  with (23b) gives in the limit of

small magnetic field

$$\eta_{0,opt} = \frac{\mathbf{h}^T \cdot \left( \mathbf{H}_1^{(x)} / \tan(\theta_H) \right) \cdot \mathbf{A}_{supply,opt}^{(x)}}{\sqrt{\mathbf{h}^T \cdot \mathbf{H}_0^{(x)} \cdot \mathbf{h}} \sqrt{\left( \mathbf{A}_{supply,opt}^{(x)} \right)^T \cdot \mathbf{H}_0^{(x)} \cdot \mathbf{A}_{supply,opt}^{(x)}}} \quad (59)$$

We will refer to (59) in **Appendix B**. However, for numerical optimization we use an alternative equation. To this end we insert (57) and (23b) into (55), and we get

$$\eta_{0,opt}^2 = \frac{\left( \mathbf{A}_{supply,opt}^{(x)} \right)^T \cdot \left( \bar{\mathbf{X}} + \left( \mathbf{H}_0^{(x)} \right)^T \cdot \mathbf{X} \right) \cdot \frac{\mathbf{R}_1^T}{\tan(\theta_H)} \cdot \mathbf{G}_0 \cdot \frac{\mathbf{R}_1}{\tan(\theta_H)} \cdot \left( \bar{\mathbf{X}} + \mathbf{X} \cdot \mathbf{H}_0^{(x)} \right) \cdot \mathbf{A}_{supply,opt}^{(x)}}{\left( \mathbf{A}_{supply,opt}^{(x)} \right)^T \cdot \mathbf{H}_0^{(x)} \cdot \mathbf{A}_{supply,opt}^{(x)}} \quad (60a)$$

With (26a) it holds

$$\bar{\mathbf{X}} + \mathbf{X} \cdot \mathbf{H}_0^{(x)} = \left( \bar{\mathbf{X}} + \mathbf{X} \cdot \mathbf{R}_0 \right)^{-1} \quad (60b)$$

In the denominator of (60a)  $\mathbf{H}_0^{(x)}$  is positive definite (see (23b)). Hence, we can manipulate (60a) analogous to **Appendix B** to get a Rayleigh quotient. Yet, we are not interested in the global optimum of (60a) for arbitrary  $\mathbf{A}_{supply,opt}^{(x)}$ . Instead, we look for a maximum of (60a) amongst all  $\mathbf{A}_{supply,opt}^{(x)}$  having only 1-s and 0-s, with 1-s in at least one entry indicated by  $\mathbf{X}$ . Since we have not found a closed form solution, we have to try out all possible  $\mathbf{X}$  in (60a), and for each  $\mathbf{X}$  we have to try out all possible  $\mathbf{A}_{supply,opt}^{(x)}$ . The advantage of (60a) is that we only have to compute it for a finite number of cases to find the optimum. Unfortunately, this number is huge if the Hall plate has many contacts.

**Figure 6** shows a code in MATHEMATICA, which steps through all 19 configurations of a Hall plate with four contacts and computes all noise efficiencies with (60a). The results for the Hall plate from our previous example with its resistance matrix in (56a, b) are given in **Table 1**. We note three configurations (# 3, 9, 18) with similar and large noise efficiency near 0.45. This is only 5% lower than the maximum possible noise efficiency of Hall plates with four contacts, which is  $\sqrt{2}/3 \cong 0.471$  and which is obtained for symmetrical Hall plates (see [25] [28]). Thereby the maximum noise efficiency is given for the classical configuration {2, 1, 2}, *i.e.*, contacts 1 and 3 are open and contact 2 is at supply voltage. This noise efficiency matches perfectly with our first result in case # 1 above. Due to the asymmetry of the Hall plate the coefficients on contacts 1 and 3 do not have the same magnitude. It is also interesting to note that  $h_2$  is exactly zero, whereas  $c_2$  is only small (0.003) but not zero. It means that whenever voltage is supplied at contact 2 according to **Figure 3**, we do not need to measure current there, because  $h_2 = 0$ . However, we may also supply current at contact 2 according to **Figure 1**, and then we would have to measure the voltage at contact 2, multiply it by the small values of  $c_2$  and add it to the signals from contacts 1 and 3.

In **Table 1**, configuration {0, 1, 1} in line # 3 has the second largest noise efficiency. There, contacts 1 and 4 are grounded, while contacts 2 and 3 are tied to

**Table 1.** Maximum noise efficiencies and optimum coefficient vectors obtained from the algorithm in **Figure 6** for an irregular Hall plate with  $N=4$  contacts with the resistance matrix in (56a, b). “config” means the configuration {cont1, cont2, cont3} for the three available contacts (the fourth contact is always grounded). “ $x$ ” is the number of the hybrid mode.  $A_{\text{supply, opt}}^{(x)}$  denotes the supply vector in the hybrid mode, whereby full supply voltage is applied to all contacts denoted with a “1”, while the “0”-s mean either zero voltage or zero current, depending on config.  $\eta_0$  is the noise efficiency. The six rightmost columns give the coefficient vectors  $\mathbf{c}$  and  $\mathbf{h}$ , if the circuit is implemented according to **Figure 1** or **Figure 3**, respectively. The global optimum is in line #18, but noise efficiencies in lines #3 and #9 are only slightly smaller.

#	config	$x$	$A_{\text{supply, opt}}^{(x)}$	$\eta_0$	$c_1$	$c_2$	$c_3$	$h_1$	$h_2$	$h_3$
1	{001}	7	(0, 0, 1) <sup>T</sup>	0.327510	-0.0628187	0.998025	0	-0.435343	-0.805412	-0.402229
2	{010}	7	(0, 1, 0) <sup>T</sup>	0.338385	0.654278	0	-0.756254	-0.801024	-0.00583891	0.598604
3	{011}	7	(0, 1, 1) <sup>T</sup>	0.445647	0.493397	0.615044	-0.615044	-0.741122	-0.669613	-0.0485418
4	{012}	3	(0, 1, 0) <sup>T</sup>	0.412759	0.608926	0.317462	-0.72693	-0.637599	-0.348361	-0.687104
5	{021}	5	(0, 0, 1) <sup>T</sup>	0.403891	0.307932	0.854616	-0.418102	-0.666542	0.707009	-0.236349
6	{100}	7	(1, 0, 0) <sup>T</sup>	0.347308	0	-0.997364	0.0725615	0.466202	0.801201	0.375145
7	{101}	7	(1, 0, 1) <sup>T</sup>	0.041047	-0.389561	0.834556	0.389561	-0.219468	-0.799294	-0.55943
8	{102}	3	(1, 0, 0) <sup>T</sup>	0.304065	-0.00970987	-0.996442	0.0837177	0.506047	0.860215	0.0628248
9	{110}	7	(1, 1, 0) <sup>T</sup>	0.443810	0.56138	-0.56138	-0.608034	-0.0561225	0.718156	0.693615
10	{111}	7	(1, 1, 1) <sup>T</sup>	0.339706	0.646483	0.108666	-0.75515	-0.860281	-0.196367	0.470486
11	{112}	3	(1, 1, 0) <sup>T</sup>	0.417499	0.643481	-0.242134	-0.726157	-0.387323	0.326488	-0.862199
12	{120}	5	(1, 0, 0) <sup>T</sup>	0.412272	0.331226	-0.888269	-0.318226	0.295321	-0.764295	0.573271
13	{121}	5	(1, 0, 1) <sup>T</sup>	0.293825	0.644369	0.12723	-0.754056	-0.871548	0.193144	0.450665
14	{122}	1	(1, 0, 0) <sup>T</sup>	0.348047	0.539373	-0.611465	-0.578954	0	-0.726147	-0.687539
15	{201}	6	(0, 0, 1) <sup>T</sup>	0.281115	-0.0739121	0.997182	0.0128837	-0.0574435	-0.89118	-0.449998
16	{210}	6	(0, 1, 0) <sup>T</sup>	0.404698	0.632018	-0.316174	-0.707522	0.702803	0.40055	0.587901
17	{211}	6	(0, 1, 1) <sup>T</sup>	0.390947	0.609242	0.316226	-0.727204	0.831664	-0.501166	0.239097
18	{212}	2	(0, 1, 0) <sup>T</sup>	0.446151	0.654388	-0.00314656	-0.756152	0.654392	0	-0.756156
19	{221}	4	(0, 0, 1) <sup>T</sup>	0.338077	0.525055	0.552784	-0.647107	0.688688	0.725058	0

supply voltage. According to **Figure 3**, currents are measured at all contacts with ideal transformers, yet the one at contact 3 has a small coefficient  $h_3 = -0.05$ . Alternatively, we could work with current sources only. Then, we need specific supply currents  $\mathbf{I}_{\text{supply}} = V_{\text{supply}} \mathbf{R}_0^{-1} \cdot (0, 1, 1)^T$  to achieve potentials near  $V_{\text{supply}}$  at contacts 2 and 3 and near ground at contact 1 (not given in **Table 1**), and then we would have to sample the potentials at all contacts with weighing factors given by  $\mathbf{c}$ , whereby  $c_3 = -c_2$  according to **Table 1**.

The third largest noise efficiency is achieved with configuration {1, 1, 0} in line # 9 of **Table 1**. This case is similar to # 3 when we swap contacts 1 and 3 (exact mirror symmetry is spoiled by the asymmetry of the Hall plate itself).

As a second numerical example we consider a regular Hall plate with  $N = 5$  contacts. “Regular” means that all contacts are  $36^\circ$  large and spaced apart by  $36^\circ$ . With the method of [14] we get the following resistance matrices at weak

```
(* Testing all hybrid configurations "ground/Vsupply/open" at the contacts:

The algorithm uses the following input data:
Rmatrix ... 3x3 resistance matrix of
Hall plate with 4 contacts at small Hall angle thetaH
Rmatrix0 ... same matrix at zero magnetic field
thetaH ... Hall angle
n = 4 ... number of contacts
*)
cplus[l1_] := Sum[l1[[i]], {i, Length[l1]}]
loopcount = 0;
etax0 = Table[0, {i, 3^(n-1) - 2^(n-1)}];
Gmatrix0 = Inverse[Rmatrix0];
sqrtGmatrix0 = MatrixPower[Gmatrix0, 1/2];
Rltg = (Rmatrix - Rmatrix0) / Tan[thetaH];
Mmx1 = sqrtGmatrix0.Rltg;
Mmx2 = Gmatrix0.Rltg;
Do[Do[Do[If[cont1 == 1 || cont2 == 1 || cont3 == 1,
loopcount = loopcount + 1;
x =
If[cont1 != 2, 1, 0] * 2^0 + If[cont2 != 2, 1, 0] * 2^1 + If[cont3 != 2, 1, 0] * 2^2;
xbin = Reverse[IntegerDigits[x, 2, n-1]];
X = DiagonalMatrix[xbin];
Xq = IdentityMatrix[n-1] - X;
inversematrix = Inverse[Xq + X.Rmatrix0];
Hx0 = (Xq.Rmatrix0 + X).inversematrix;
Axsupply = {KroneckerDelta[cont1, 1],
KroneckerDelta[cont2, 1], KroneckerDelta[cont3, 1]};
vector1 = Mmx1.inversematrix.Axsupply;
etax0[[loopcount]] =
Sqrt[cplus[vector1 * vector1] / cplus[Axsupply * (Hx0.Axsupply)]];
Isup = (Xq + X.Hx0).Axsupply;
c = Mmx2.Isup;
dl = Rmatrix0.c;
hl = Inverse[Xq - X.Transpose[Hx0]].c;
hl = hl / Sqrt[cplus[hl * hl]];
dl = dl / Sqrt[cplus[dl * dl]];
c = c / Sqrt[cplus[c * c]];
Isup = Isup / Sqrt[cplus[Isup * Isup]];
Print["# ", loopcount, " config= ", {cont1, cont2, cont3}, " x= ", x,
"Axsupply= ", Axsupply, " eta0x= ", N[etax0[[loopcount]]],
"d = ", N[dl], " c= ", N[c], " h= ", N[hl], " Isupply= ", N[Isup]],
{cont3, 0, 2}], {cont2, 0, 2}], {cont1, 0, 2}];
Print["number of loops = ", loopcount]
```

**Figure 6.** Algorithm programmed in MATHEMATICA to step through all hybrid configurations (with 0 V,  $V_{supply}$  or zero current at the contacts) to search for the global maximum of the noise efficiency. The contact configuration is given by {cont1, cont2, cont3} for the three free contacts of a Hall plate with  $N=4$  contacts.

magnetic field and for a sheet resistance of  $1 \Omega$  (note the symmetry of both matrices due to the symmetry of the regular Hall plate)

$$R_0 = \begin{pmatrix} 1.231070 & 0.760845 & 0.615537 & 0.470228 \\ 0.760845 & 1.521690 & 0.906154 & 0.615537 \\ 0.615537 & 0.906154 & 1.521690 & 0.760845 \\ 0.470228 & 0.615537 & 0.760845 & 1.231070 \end{pmatrix} \tag{61a}$$

$$\lim_{\theta_H \rightarrow 0} \frac{R_1}{\tan(\theta_H)} = \begin{pmatrix} 0 & 0.338115 & 0.361393 & 0.338115 \\ -0.338115 & 0 & 0.361393 & 0.361393 \\ -0.361393 & -0.361393 & 0 & 0.338115 \\ -0.338115 & -0.361393 & -0.338115 & 0 \end{pmatrix} \tag{61b}$$

The largest noise efficiency is  $\eta_0 = 0.548867$ , and it is obtained for the seven optimum configurations in lines # 11, 17, 18, 35, 55, 57, 58 of **Table 2**. This suggests that regular Hall plates have several identical optima, whereas irregular Hall plates tend to have a group of configurations with similar noise optimum but only one of them is the global optimum.

All seven optimum configurations are mirror-symmetric, yet only in three of these configurations the axis of mirror symmetry goes through the grounded

**Table 2.** Maximum noise efficiencies  $\eta_0$  and optimum coefficient vectors  $\mathbf{c}$  and  $\mathbf{h}$  obtained from the algorithm in **Figure 6**, adapted for a regular Hall plate with  $N=5$  contacts, with the resistance matrix in (61a, b). The symbols are identical to **Table 1**. From all 65 possible configurations only the ones with maximum noise efficiency are given.

#	config	$x$	$A_{\text{supply, opt}}^{(x)}$	$\eta_0$					
11	{0112}	7	$(0, 1, 1, 0)^T$	0.548867					
17	{0211}	13	$(0, 0, 1, 1)^T$	0.548867					
18	{0212}	5	$(0, 0, 1, 0)^T$	0.548867					
35	{1120}	11	$(1, 1, 0, 0)^T$	0.548867					
55	{2110}	14	$(0, 1, 1, 0)^T$	0.548867					
57	{2112}	6	$(0, 1, 1, 0)^T$	0.548867					
58	{2120}	10	$(0, 1, 0, 0)^T$	0.548867					
#	$c_1$	$c_2$	$c_3$	$c_4$	$h_1$	$h_2$	$h_3$	$h_4$	
11	0.550373	0.550373	-0.266029	-0.568688	-0.605115	-0.605115	0	-0.517371	
17	0.30359	0.648983	0.30359	-0.628082	-0.605115	0.517371	-0.605115	0	
18	0.308372	0.672647	0	-0.672647	-0.500883	0.585831	-0.250442	-0.585831	
35	0.628082	-0.30359	-0.648983	-0.30359	0	0.605115	-0.517371	0.605115	
55	0.568688	0.266029	-0.550373	-0.550373	0.517371	0	0.605115	0.605115	
57	0.642779	0.294679	-0.294679	-0.642779	0.650186	-0.277954	0.277954	-0.650186	
58	0.672647	0	-0.672647	-0.308372	0.585831	0.250442	-0.585831	0.500883	

contact. Configuration {2112} in line # 57 has an axis of mirror-symmetry through the grounded contact 5: contacts 2 and 3 are connected to supply voltage while contacts 1 and 4 are open. Both coefficient vectors  $\mathbf{c}$  and  $\mathbf{h}$  reflect this symmetry.

Conversely, configuration {0211} in line # 17 has a symmetry axis through contact 2: contact 1 is at ground, contact 2 is open, and contacts 3 and 4 are connected to supply voltage. If we implement this configuration according to **Figure 3** we apply  $V_{\text{supply}}$  to contacts 1, 3, and 4, while contact 2 is left open. Then we have to measure current at contacts 1 and 3 and we can skip current measurement at contact 4, because  $h_4 = 0$ . And we need to measure voltage at contact 2 with a different coefficient than the two current measurements ( $h_2 \neq h_1 = h_3$ ). Alternatively, we can implement the same configuration in pure voltage mode according to **Figure 1**. Then the supply currents are given by (22b) and (23a) as  $\mathbf{I}_{\text{supply}} = V_{\text{supply}} (\bar{\mathbf{X}} + \mathbf{X} \cdot \mathbf{H}_0^{(13)}) \cdot (0, 0, 1, 1)^T$ , where  $\bar{\mathbf{X}}$  and  $\mathbf{X}$  are evaluated for hybrid mode number  $x = 13$ . Then the coefficients  $\mathbf{c}$  apply according to **Section 3.2**. All four coefficients are significant, whereby the voltage at the fourth contact is subtracted from all others, which is again surprising (because out of the stomach feeling one would expect a more efficient signal from a regular Hall plate if two contacts are subtracted from the other two).

To sum up, we see that there are many solutions for best noise performance

for general asymmetric Hall plates—and regular Hall plates have even more optimum solutions. With our theory of hybrid operating modes from **Sections 3** and **4** it is straightforward to find all of them, to keep the survey, and to select the one which fits best to the practical needs of the specific technology at hand.

### 6. The Ultimate Noise Efficiency of Hall Plates

Here we consider the noise optimization if only the power in the Hall plate is accounted for (“lossless bias”, no dissipation in the bias circuit). **Figure 7** shows a circuit, where supply voltages and currents are coupled into the Hall plate via ideal transformers and gyrators. Since ideal transformers and gyrators are passive and lossless, the power of the circuit becomes identical to the power of the Hall plate. In such a case we denote the noise efficiency by a prime  $\eta'$ . We have two coefficient vectors:  $\mathbf{a}$  for the power coupling and  $\mathbf{h}$  for the signals.

We consider the general hybrid operating mode number  $x$ . The output conductance seen by the ampere-meter in **Figure 7** is  $G_{\text{out}} = \mathbf{h}^T \cdot \mathbf{H}^{(x)} \cdot \mathbf{h}$ . If we plug **Figure 7** into the difference-field circuit of **Figure 4** the output signal is  $I_{\text{diff}} = \mathbf{h}^T \cdot (\mathbf{H}^{(x)} - \mathbf{H}^{(x)}(-B_{\perp})) \cdot \mathbf{a}$ . Then the power is  $P_{\text{diff}} = 2P_{\text{Hall}} = \mathbf{a}^T \cdot (\mathbf{H}^{(x)} + \mathbf{H}^{(x)}(-B_{\perp})) \cdot \mathbf{a}$ . With (6) we get the noise efficiency for a Hall plate embedded in this lossless Hall bias circuit in the limit of small magnetic field.

$$\eta'_0 = \frac{\mathbf{h}^T \cdot (\mathbf{H}_1^{(x)} / \tan(\theta_H)) \cdot \mathbf{a}}{\sqrt{\mathbf{h}^T \cdot \mathbf{H}_0^{(x)} \cdot \mathbf{h}} \sqrt{\mathbf{a}^T \cdot \mathbf{H}_0^{(x)} \cdot \mathbf{a}}} \tag{62a}$$

(62a) has the same shape as (59) if we replace  $A_{\text{supply,opt}}^{(x)}$  by  $\mathbf{a}$ . However,  $A_{\text{supply,opt}}^{(x)}$  has only zeros and ones, whereas  $\mathbf{a}$  can be any real valued vector. Thus, the definition space of  $\mathbf{a}$  comprises all possible values of  $A_{\text{supply,opt}}^{(x)}$  and therefore the global maximum of  $\eta'_0$  cannot be smaller than the one of  $\eta_0$ .

$$\max_{\mathbf{a}, \mathbf{h}} \eta'_0 \geq \max_{A, \mathbf{h}} \eta_0 \tag{62b}$$

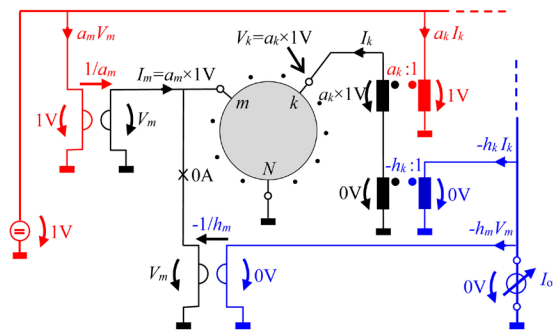


**Figure 7.** General Hall plate in hybrid operating mode with power coupled lossless via ideal transformers and gyrators. The power dissipated by the circuit is identical to the power in the Hall plate. This is the most economical way to supply a multi-contact Hall plate with electrical energy. The coefficients for the power coupling are  $\mathbf{a}$  (in red), the coefficients for the signals are  $\mathbf{h}$  (in blue). Power and signal transformers are connected in series to a contact, while power and signal gyrators are connected in parallel to a contact.

If  $\mathbf{a} = (\mathbf{X} - \bar{\mathbf{X}}) \cdot \mathbf{h}$  it follows  $\eta'_0 = 0$  because  $\mathbf{H}_1^{(x)} \cdot (\mathbf{X} - \bar{\mathbf{X}})$  is odd symmetric (cf. (58b)). Then, the total Hall signal  $I_{\text{out}}$  vanishes.

Analogous to (34) we set  $\mathbf{a} = (\mathbf{X} \cdot \mathbf{R}_0 + \bar{\mathbf{X}}) \cdot \mathbf{I}_{\text{supply}}^{(0)}$ . Then the powers at all contacts remain constant versus  $x$ , i.e., in all hybrid operating modes the same power vector  $\mathbf{P}$  is applied to the Hall plate

$$\begin{aligned} \mathbf{P} &= \text{diag}\{\mathbf{a}\} \cdot \mathbf{H}_0^{(x)} \cdot \mathbf{a} \\ &= \text{diag}\left\{\mathbf{X} \cdot \mathbf{R}_0 \cdot \mathbf{I}_{\text{supply}}^{(0)} + \bar{\mathbf{X}} \cdot \mathbf{I}_{\text{supply}}^{(0)}\right\} \cdot \mathbf{H}_0^{(x)} \cdot (\mathbf{X} \cdot \mathbf{R}_0 + \bar{\mathbf{X}}) \cdot \mathbf{I}_{\text{supply}}^{(0)} \\ &= \left(\text{diag}\left\{\mathbf{R}_0 \cdot \mathbf{I}_{\text{supply}}^{(0)}\right\} \cdot \mathbf{X} + \text{diag}\left\{\mathbf{I}_{\text{supply}}^{(0)}\right\} \cdot \bar{\mathbf{X}}\right) \cdot (\bar{\mathbf{X}} \cdot \mathbf{R}_0 + \mathbf{X}) \cdot \mathbf{I}_{\text{supply}}^{(0)} \quad (63a) \\ &= \mathbf{X} \cdot \text{diag}\left\{\mathbf{R}_0 \cdot \mathbf{I}_{\text{supply}}^{(0)}\right\} \cdot \mathbf{I}_{\text{supply}}^{(0)} + \bar{\mathbf{X}} \cdot \text{diag}\left\{\mathbf{I}_{\text{supply}}^{(0)}\right\} \cdot \mathbf{R}_0 \cdot \mathbf{I}_{\text{supply}}^{(0)} \\ &= (\mathbf{X} + \bar{\mathbf{X}}) \cdot \text{diag}\left\{\mathbf{I}_{\text{supply}}^{(0)}\right\} \cdot \mathbf{R}_0 \cdot \mathbf{I}_{\text{supply}}^{(0)} = \text{diag}\left\{\mathbf{I}_{\text{supply}}^{(0)}\right\} \cdot \mathbf{R}_0 \cdot \mathbf{I}_{\text{supply}}^{(0)} \end{aligned}$$

In (63a) we used (38a) and (21b-d). (63a) also means that the power dissipated in the Hall plate is identical in all hybrid operating modes.

$$P_{\text{Hall}} = \mathbf{u}^T \cdot \mathbf{P} = \mathbf{a}^T \cdot \mathbf{H}_0^{(x)} \cdot \mathbf{a} = \left(\mathbf{I}_{\text{supply}}^{(0)}\right)^T \cdot \mathbf{R}_0 \cdot \mathbf{I}_{\text{supply}}^{(0)} \quad (63b)$$

The transformations (39)-(44) and (48) say  $\mathbf{h}^T \cdot \mathbf{H}_0^{(x)} \cdot \mathbf{h} = \mathbf{c}^T \cdot \mathbf{Q} \cdot \mathbf{c} = \mathbf{c}^T \cdot \mathbf{R}_0 \cdot \mathbf{c}$ , which means that the output conductance in hybrid mode (29) is identical to the output resistance in voltage mode (9). Using this and inserting (40a) and (63b) into (39) gives

$$\eta'_0 = \frac{\mathbf{c}^T \cdot (\mathbf{R}_1 / \tan(\theta_H)) \cdot \mathbf{I}_{\text{supply}}^{(0)}}{\sqrt{\left(\mathbf{I}_{\text{supply}}^{(0)}\right)^T \cdot \mathbf{R}_0 \cdot \mathbf{I}_{\text{supply}}^{(0)}} \sqrt{\mathbf{c}^T \cdot \mathbf{R}_0 \cdot \mathbf{c}}} \quad (63c)$$

(63c) is analogous to (49), and it shows that also for lossless bias the noise efficiency  $\eta'_0$  is identical for all hybrid operating modes.

The maximization of  $\eta'_0$  in (63c) is a problem, which has been solved in statistics, where it is known as canonical-correlation analysis [29] [30]. Its solution comprises three steps: first,  $\mathbf{R}_0$  is factorized such that the terms in the denominator become norms of vectors, second, the numerator is interpreted as a product of two vectors and the Cauchy-Schwartz inequality is applied, and in a third step the result of these manipulations is identified as a Rayleigh quotient with a known maximum.

*Step 1:*

It holds  $\left(\mathbf{I}_{\text{supply}}^{(0)}\right)^T \cdot \mathbf{R}_0 \cdot \mathbf{I}_{\text{supply}}^{(0)} > 0$ , because the power dissipation is positive for any real-valued non-vanishing current  $\mathbf{I}_{\text{supply}}^{(0)}$ . In other words,  $\mathbf{R}_0$  is positive definite. Therefore, it has a *unique* positive definite square root  $\mathbf{R}_0^{1/2}$  which is defined by

$$\mathbf{R}_0 = \mathbf{R}_0^{1/2} \cdot \mathbf{R}_0^{1/2} \quad (64)$$

$\mathbf{R}_0$  and  $\mathbf{R}_0^{1/2}$  are symmetric. One way to compute the square root is to diagonalize  $\mathbf{R}_0 = \mathbf{E} \cdot \mathbf{D} \cdot \mathbf{E}^{-1}$ , where  $\mathbf{D}$  is an  $(N - 1) \times (N - 1)$  diagonal matrix with the  $N - 1$  eigenvalues of  $\mathbf{R}_0$  on its main diagonal, and the columns of  $\mathbf{E}$

are the corresponding eigenvectors (both in the same order—usually one starts with the largest eigenvalue in the first column). Since  $\mathbf{R}_0$  is positive definite, the entries of  $\mathbf{D}$  are positive. Since  $\mathbf{R}_0$  is symmetric,  $\mathbf{E}$  is unitary  $\mathbf{E}^{-1} = \mathbf{E}^T$ . Then it holds

$$\mathbf{R}_0^{1/2} = \mathbf{E} \cdot \mathbf{D}^{1/2} \cdot \mathbf{E}^{-1} \tag{65}$$

where the entries of  $\mathbf{D}^{1/2}$  are the positive square roots of the entries of  $\mathbf{D}$ . (65) can be proven by inserting it into (64). Since  $\mathbf{D}$  has only real entries and the square root can be positive or negative, there are  $2^{N-1}$  solutions for  $\mathbf{D}^{1/2}$ . Yet, only one solution has all positive entries and therefore it is positive definite. In Mathematica the square root of a matrix is computed by MatrixPower [ $\mathbf{R}_0$ , 1/2] (see Figure 6).

Now, that we know a unique  $\mathbf{R}_0^{1/2}$  exists, we can use it for our optimization problem. We define new vectors

$$\mathbf{v}_1 = \mathbf{R}_0^{1/2} \cdot \mathbf{I}_{\text{supply}}^{(0)} \quad \text{and} \quad \mathbf{v}_2 = \mathbf{R}_0^{1/2} \cdot \mathbf{c} \tag{66}$$

and insert this into (63c). This gives

$$\eta'_0 = \frac{\mathbf{v}_2^T \cdot \mathbf{M} \cdot \mathbf{v}_1}{\sqrt{\mathbf{v}_1^T \cdot \mathbf{v}_1} \sqrt{\mathbf{v}_2^T \cdot \mathbf{v}_2}} \quad \text{with} \quad \mathbf{M} = \mathbf{R}_0^{-1/2} \cdot \frac{\mathbf{R}_1}{\tan(\theta_H)} \cdot \mathbf{R}_0^{-1/2} \tag{67}$$

From (58a) it follows  $\mathbf{M}^T = -\mathbf{M}$ , i.e.,  $\mathbf{M}$  is skew-symmetric.

Step 2:

We apply the Cauchy-Schwartz inequality to the numerator of (67).

$$(\mathbf{v}_2^T \cdot \mathbf{M}) \cdot \mathbf{v}_1 \leq \sqrt{\mathbf{v}_2^T \cdot \mathbf{M} \cdot (\mathbf{v}_2^T \cdot \mathbf{M})^T} \times \sqrt{\mathbf{v}_1^T \cdot \mathbf{v}_1} \tag{68}$$

The numerator becomes largest if the equal sign holds. Then, the two vectors are parallel (colinear)

$$\mathbf{v}_1 = s \mathbf{M}^T \cdot \mathbf{v}_2 \tag{69}$$

where  $s \neq 0$  is some real-valued scalar factor. Inserting (69) into (67) gives

$$(\eta'_0)^2 \leq \frac{\mathbf{v}_2^T \cdot \mathbf{M} \cdot \mathbf{M}^T \cdot \mathbf{v}_2}{\mathbf{v}_2^T \cdot \mathbf{v}_2} \tag{70}$$

Step 3:

The RHS of (70) is the Rayleigh quotient of the matrix  $\mathbf{M} \cdot \mathbf{M}^T$  [31] [32]. It is known that this quotient becomes largest when  $\mathbf{v}_2$  is the eigenvector of  $\mathbf{M} \cdot \mathbf{M}^T$  that corresponds to the largest eigenvalue of  $\mathbf{M} \cdot \mathbf{M}^T$ . Then the Rayleigh quotient is equal to the largest eigenvalue. We can get a relation between eigenvalues of  $\mathbf{M} \cdot \mathbf{M}^T$  and  $\mathbf{M}$  by diagonalizing both matrices.

$$\mathbf{M} = \mathbf{E}_M \cdot \mathbf{D}_M \cdot \mathbf{E}_M^{-1} \Rightarrow \mathbf{M} \cdot \mathbf{M}^T = -\mathbf{M} \cdot \mathbf{M} = -\mathbf{E}_M \cdot \mathbf{D}_M^2 \cdot \mathbf{E}_M^{-1} \tag{71}$$

$\mathbf{M} \cdot \mathbf{M}^T$  is symmetric. With (70) it is positive semi-definite, and therefore it has non-negative eigenvalues. Thus, the entries on the main diagonal of  $-\mathbf{D}_M^2$  are non-negative. Consequently, the eigenvalues of  $\mathbf{M}$  are pure imaginary or zero. (71) shows also that  $\mathbf{M}$  and  $\mathbf{M} \cdot \mathbf{M}^T$  have the same eigenvectors. These

are known properties of skew-symmetric matrices [33].

Summing up these findings, the maximum noise efficiency  $\eta'_0$  is equal to the largest magnitude of the eigenvalues of the matrix  $\mathbf{M} = \mathbf{G}_0^{1/2} \cdot (\mathbf{R}_1 / \tan(\theta_H)) \cdot \mathbf{G}_0^{1/2}$ . If we denote the eigenvector corresponding to this largest eigenvalue with  $\mathbf{v}_2$  we need the following coefficient vectors and current vectors to achieve this best noise performance.

$$\mathbf{c}_{opt} = \mathbf{G}_0^{1/2} \cdot \mathbf{v}_2 \quad \text{and} \quad \mathbf{I}_{supply,opt}^{(0)} = -s\mathbf{G}_0 \cdot (\mathbf{R}_1 / \tan(\theta_H)) \cdot \mathbf{c}_{opt} \quad (72)$$

With  $\mathbf{M}$  and (72) we get the best possible noise efficiency and the respective coefficients and currents in closed form, without a time consuming and error prone numerical optimization. Note that  $\mathbf{M}$  is dimension-less, which is consistent with our introductory statement, that the noise efficiency does not depend on any physical quantity (see (6)).

Finally we compare  $\eta_0$  and  $\eta'_0$  for a regular Hall plate with  $N = 40$  contacts. In [25] we found a current pattern for  $\eta_0 = 0.89152$  (see the first plot (a) in Figure 8). However, with (60a) we found a slightly larger noise efficiency  $\eta_0 = 0.91876$ , which we have overlooked in [25] (see the second plot (b) in Figure 8). With the eigenvalues of  $\mathbf{M}$  the optimization of (63c) gives  $\eta'_0 = 0.94239$  (see the third plot (c) in Figure 8). Thus, the difference in optimum noise efficiency between lossless and lossy bias is only moderate ( $\max \eta'_0$  is only 2.6% larger than  $\max \eta_0$ ). Yet, the optimum current patterns and coefficient patterns are markedly different for both cases, as it is apparent in Figure 8. For maximum  $\eta_0$  (“lossy bias”) the currents are such, that the voltages at zero magnetic field are 0 V for contacts 1, 2, 3, 4, 5, 36, 37, 38, 39, 40, and they are at the positive supply voltage for contacts 16 to 25. No current flows through all other contacts at zero magnetic field. Conversely, for maximum  $\eta'_0$  (“lossless bias”) the current pattern is approximately sinusoidal with largest negative current through contacts 1 and 40, and largest positive current through contacts 20 and 21. Thus, currents flow through all contacts at zero magnetic field. The patterns of the optimum coefficients are also different: for maximum  $\eta_0$  the pattern of coefficients  $\mathbf{c}$  is roughly pulse shaped with strong overshoot at contacts 6, 15, 26, 35, whereas for maximum  $\eta'_0$  they are sinusoidally distributed and in quadrature (shifted by  $90^\circ$ , which is 10 contacts) to the current pattern.

In practice the effort of implementing the circuit for optimum lossless bias ( $\eta'_0$ ) is much larger than the effort for optimum lossy bias ( $\eta_0$ ). For optimum lossless bias only two of the forty currents are equal, and only two of the forty coefficients are equal. Thus, the circuit has to provide 20 current sources and 20 preamps (if the coefficients are defined by the preamps), and it needs  $40^2 = 1600$  switches that connect each contact to all current sources and all preamps during a spinning current scheme. For the lossy bias there are only 10 current sources and 20 coefficients, which requires four times fewer switches. Moreover, several coefficients are nearly zero, and other coefficients and currents are nearly identical. Therefore, one can approximate the optimum patterns with only three different positive coefficients (the negative ones can be done simply by inverting

the preamp outputs) and two positive and two negative currents (for zero

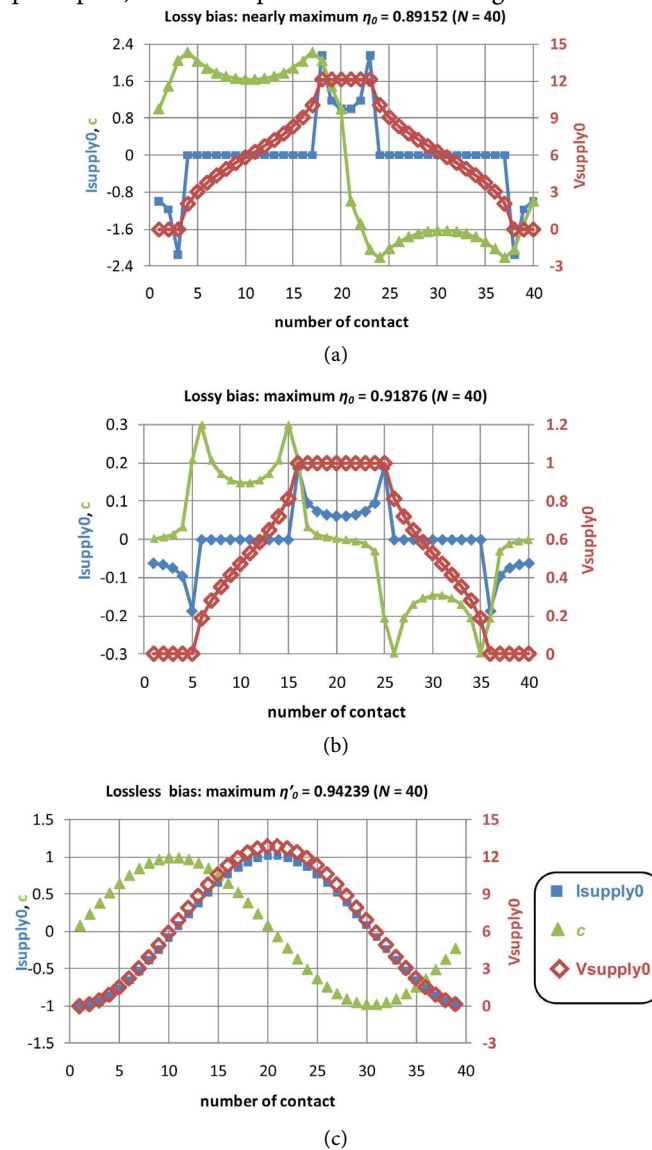


**Figure 8.** ((a)-(c)) Results of optimizations for the maximum noise efficiency of a regular Hall plate with 40 contacts: Patterns of supply current, supply voltage, and coefficients  $c$ . Figures ((a), (b)) show patterns for large  $\eta_0$  according to (49) (including the power dissipated in the MOS pass devices: “lossy bias”). Thereby, (a) is close to optimum noise efficiency, but still less than the true optimum in (b). (c) shows patterns for maximum  $\eta'_0$  in (63c) (with lossless Hall supply circuit). Current and coefficient vectors are not normalized in the upper plots—in the lower plot they are normalized to values in the interval  $[-1, 1]$ . The legend of (c) applies also to (a) and (b).

current we need no additional switch). This needs “only”  $40 \times 7 = 280$  small switches. Obviously, there is plenty of room for future work to optimize the circuit topology and the layout of the switches and the preamps.

On the other hand, the power density, the electric field, and the temperature are more homogeneous in the case of optimum lossless bias, which should give smaller residual offset errors after spinning current schemes are applied—but

this is beyond the scope of our linear theory. **Figure 9** shows the power density

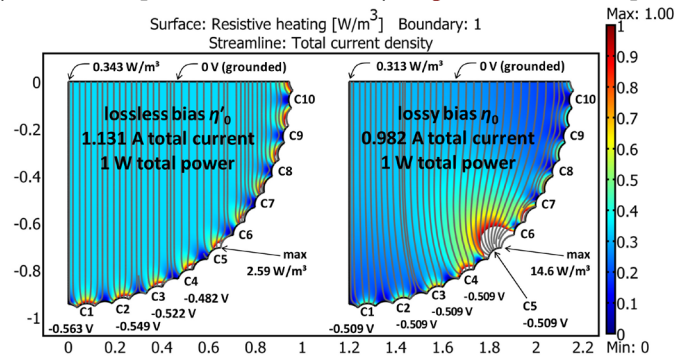


**Figure 9.** Current flow lines and power density in a regular CAPD Hall plate with 40 contacts at zero magnetic field (as obtained by a finite element simulation). Only a quarter of the symmetric Hall plate is shown. In the left plot the sinusoidal current pattern for maximum  $\eta'_0$  was assumed (case “lossless bias”). In the right plot the current pattern for maximum  $\eta_0$  was assumed (case “lossy bias”). Both current patterns were scaled to dissipate 1 W in the Hall plate. All white regions within the Hall plates denote power densities in excess of  $1 \text{ W/m}^3$ , where the color coding was clipped. The right Hall plate has much less homogeneous power distribution than the left one.

in a quarter of a Hall plate with currents according to maximum  $\eta'_0$  and  $\eta_0$ . The displayed data comes from a finite element simulation with the commercial program COMSOL. A 2D static electricity model (“emdc”) was used. It assumes a Hall plate thickness of 1 m, a specific conductivity of 1 S/m, and zero magnetic field. The Hall plate has a perimeter that consists of 80 equal circular arcs, where every second one is a contact. The circular arc polygonal domain (CAPD) was used, because it avoids singularities of the power density when the arcs intersect at  $90^\circ$ . Note that the CAPD in **Figure 9** has the same resistance matrix as the regular circular Hall plate in **Figure 8**, because we can map one onto the other by a conformal mapping. With the same resistance matrix, also the same optimal current and coefficient vectors apply. Due to symmetry, only a quarter of the Hall plate needs to be modeled. We defined the potential on the upper edge as 0 V, and we applied currents at all contacts according to the optimum patterns in **Figure 8**. Thereby the currents were scaled such that the total dissipated power was 1 W in both cases. The displayed power densities in **Figure 9** are clipped at  $1 \text{ W/m}^3$  for the sake of visibility. Obviously, the power density in the left plot is more homogeneous. In the right plot (“lossy bias”) the power density at the right vertex of contact 5 has its largest value of  $14.6 \text{ W/m}^3$ , which is 47 times larger than in the major central portion of the Hall plate. According to the second plot in **Figure 8**, contact 5 also carries by far the strongest current. Also in the left plot in **Figure 9** (“lossless bias”) the power density has its maximum at the right vertex of contact 5, but there it is only  $2.59 \text{ W/m}^3$ , which is only 7.6 times larger than in the major central portion.

## 7. Conclusions

In this work we have introduced hybrid operating modes of Hall plates with N

contacts. Special cases are conventional voltage and current operating modes. We invented a counting scheme that labels all hybrid operating modes by an integer number  $x$  ranging from 0 to  $2^{N-1} - 1$ . The hybrid matrix relates input and output quantities of Hall plates in hybrid operating modes, and it is linked via  $x$  to the definite resistance matrix. The output signals of a Hall plate in hybrid operating mode are voltages and currents, and in a theoretical circuit they are extracted via passive lossless devices, ideal transformers and gyrators. Of course in practice one will use active circuits such as amplifiers and trans-conductance amplifiers. The total output signal is a linear combination of all signals from all contacts, with coefficients that need to be optimized for smallest noise. We defined the noise efficiency at weak magnetic field as the relevant figure of merit. It is the signal to thermal noise ratio normalized to the Hall angle, the temperature, the observation bandwidth, and the dissipated power. It was proven rigorously, that the noise efficiency in all hybrid operating modes is the same, provided that the supply voltages and currents and the coefficients remain the same. If the optimum supply quantities and coefficients for maximum noise efficiency are found in one hybrid operating mode, we can readily compute supply quantities and coefficients in all other hybrid operating modes to render the same noise efficiency.

We also mentioned a hypothesis, that maximum noise efficiency is obtained whenever the following condition holds for all contacts at zero applied magnetic field: either the potential is zero or  $V_{\text{supply}}$  (=voltage of the power supply circuit that supplies the Hall plate and its circuit), or the current is zero.

At weak magnetic field, the best noise efficiency, which we can get out of a Hall plate, is identical to the largest eigenvalue of the dimension-less matrix  $M = R_0^{-1/2} \cdot (R_1 / \tan(\theta_H)) \cdot R_0^{-1/2}$ , which is a function of the even ( $R_0$ ) and odd ( $R_1$ ) parts of the resistance matrix.

By way of numerical examples we showed that regular Hall plates have several configurations with highest noise efficiency, whereas irregular Hall plates are more likely to have a global optimum, which is only slightly larger than several other near-optima.

The decisive benefit of our theory is, that it outputs the optimum design parameters of Hall sensor circuits, *i.e.*, the optimum supply currents and voltages and the optimum coefficients, for any kind of Hall plate, as long as we know its resistance matrix (which can be measured easily). We do not need to know any geometrical or technological details of the Hall plate. It only takes a small numerical optimization algorithm. Moreover, the theory returns a value for the noise efficiency, and by comparison with values published in [25] we know immediately, how close the Hall plate at hand is to the theoretical noise limit. The theory can be applied to classical Hall plates, and also to Vertical Hall effect devices.

## Conflicts of Interest

The author declares no conflicts of interest regarding the publication of this pa-

per.

## References

- [1] Schott, C. and Popovic, R.S. (1997) Linearizing Integrated Hall Devices. *Proceedings of International Solid State Sensors and Actuators Conference*, Vol. 1, 393-396.
- [2] Midgley, D. (1960) The Possibility of a Self-Sustaining Corbino Disk. *Nature*, **186**, 377. <https://doi.org/10.1038/186377a0>
- [3] Johnson, H.H. and Midgley, D. (1962) The Corbino Disc and Its Self-Magnetic Field. *Proceedings of the IEE Part B: Electronic and Communication Engineering*, **109**, 283-286. <https://doi.org/10.1049/pi-b-2.1962.0199>
- [4] Boiko, B.B., Sobol, V.R., Mazurenko, O.N. and Drozd, A.A. (1996) Magnetosensitive Conductivity of Aluminum and the Advantage of Corbino Geometry. In: *Advances in Cryogenic Engineering Materials*, Springer, Boston, 1063-1069. [https://doi.org/10.1007/978-1-4757-9059-7\\_139](https://doi.org/10.1007/978-1-4757-9059-7_139)
- [5] Van der Pauw, L.J. (1961) Determination of Resistivity Tensor and Hall Tensor of Anisotropic Conductors. *Philips Research Reports*, **16**, 187-195.
- [6] Fluitman, J.H.J. (1981) On the Calculation of the Response of (Planar) Hall-Effect Devices to Inhomogeneous Magnetic Fields. *Sensors and Actuators*, **2**, 155-170. [https://doi.org/10.1016/0250-6874\(81\)80035-2](https://doi.org/10.1016/0250-6874(81)80035-2)
- [7] Ausserlechner, U. (2016) U.S. Patent No. 10,586,915. U.S. Patent and Trademark Office, Washington DC.
- [8] Ausserlechner, U. (2019) The Classical Hall Effect in Multiply-Connected Plane Regions Part II: Spiral Current Streamlines. *Journal of Applied Mathematics and Physics*, **7**, 2231-2264. <https://doi.org/10.4236/jamp.2019.710153>
- [9] Roumenin, C. and Kostov, P. (1983) Planar Hall Sensor. Bulg. Patent No 37208, Dec. 26.
- [10] Popovic, R.S. (1984) The Vertical Hall-Effect Device. *IEEE Electron Device Letters*, **5**, 357-358. <https://doi.org/10.1109/EDL.1984.25945>
- [11] Roumenin, C.S. (1992) Parallel-Field Hall Microsensors: An Overview. *Sensors and Actuators A: Physical*, **30**, 77-87. [https://doi.org/10.1016/0924-4247\(92\)80200-M](https://doi.org/10.1016/0924-4247(92)80200-M)
- [12] Ausserlechner, U. (2016) Hall Effect Devices with Three Terminals: Their Magnetic Sensitivity and Offset Cancellation Scheme. *Journal of Sensors*, **2016**, Article ID: 5625607. <https://doi.org/10.1155/2016/5625607>
- [13] Homentcovschi, D. and Bercia, R. (2018) Analytical Solution for the Electric Field in Hall Plates. *Zeitschrift für angewandte Mathematik und Physik*, **69**, 97. <https://doi.org/10.1007/s00033-018-0989-7>
- [14] Homentcovschi, D. and Murray, B.T. (2019) Explicit Resistance Matrix for a Hall Disk with Multiple Peripheral Contacts: Application to a van der Pauw Type Method for Extended Contacts. *Sensors and Actuators A: Physical*, **294**, 1-7. <https://doi.org/10.1016/j.sna.2019.04.027>
- [15] Green, M. (1961) Electrode Geometries for Which the Transverse Magnetoresistance Is Equivalent to That of a Corbino Disk. *Solid-State Electronics*, **3**, 314-316. [https://doi.org/10.1016/0038-1101\(61\)90014-4](https://doi.org/10.1016/0038-1101(61)90014-4)
- [16] Mani, R.G. and Von Klitzing, K. (1994) Temperature-Insensitive Offset Reduction in a Hall Effect Device. *Applied Physics Letters*, **64**, 3121-3123. <https://doi.org/10.1063/1.111974>

- [17] Antipov, Y. and Silvestrov, V. (2010) Hilbert Problem for a Multiply Connected Circular Domain and the Analysis of the Hall Effect in a Plate. *Quarterly of Applied Mathematics*, **68**, 563-590. <https://doi.org/10.1090/S0033-569X-2010-01189-1>
- [18] Ausserlechner, U. (2019) The Classical Hall Effect in Multiply-Connected Plane Regions Part I: Topologies with Stream Function. *Journal of Applied Mathematics and Physics*, **7**, 1968-1996. <https://doi.org/10.4236/jamp.2019.79136>
- [19] Riemann Mapping Theorem. <https://mathworld.wolfram.com/RiemannMappingTheorem.html>
- [20] Wick, R.F. (1954) Solution of the Field Problem of the Germanium Gyrator. *Journal of Applied Physics*, **25**, 741-756. <https://doi.org/10.1063/1.1721725>
- [21] Sample, H.H., Bruno, W.J., Sample, S.B. and Sichel, E.K. (1987) Reverse-Field Reciprocity for Conducting Specimens in Magnetic Fields. *Journal of Applied Physics*, **61**, 1079-1084. <https://doi.org/10.1063/1.338202>
- [22] Cornils, M. and Paul, O. (2008) Reverse-Magnetic-Field Reciprocity in Conductive Samples with Extended Contacts. *Journal of Applied Physics*, **104**, Article ID: 024505. <https://doi.org/10.1063/1.2951895>
- [23] Onsager, L. (1931) Reciprocal Relations in Irreversible Processes. II. *Physical Review*, **38**, 2265-2279. <https://doi.org/10.1103/PhysRev.37.405>
- [24] Munter, P.J.A. (1990) A Low-Offset Spinning-Current Hall Plate. *Sensors and Actuators A: Physical*, **22**, 743-746. [https://doi.org/10.1016/0924-4247\(89\)80069-X](https://doi.org/10.1016/0924-4247(89)80069-X)
- [25] Ausserlechner, U. (2020) 90% SNR Improvement with Multi-Port Hall Plates. *Journal of Applied Mathematics and Physics*, **8**, 1568-1606. <https://doi.org/10.4236/jamp.2020.88122>
- [26] Stoessel, Z. and Resch, M. (1993) Flicker Noise and Offset Suppression in Symmetric Hall Plates. *Sensors and Actuators A: Physical*, **37**, 449-452. [https://doi.org/10.1016/0924-4247\(93\)80076-S](https://doi.org/10.1016/0924-4247(93)80076-S)
- [27] Mosser, V., Matringe, N. and Haddab, Y. (2017) A Spinning Current Circuit for Hall Measurements Down to the Nanotesla Range. *IEEE Transactions on Instrumentation and Measurement*, **66**, 637-650. <https://doi.org/10.1109/TIM.2017.2649858>
- [28] Ausserlechner, U. (2017) The Signal-to-Noise Ratio and a Hidden Symmetry of Hall Plates. *Solid-State Electronics*, **135**, 14-23. <https://doi.org/10.1016/j.sse.2017.06.007>
- [29] Canonical Correlation. [https://en.wikipedia.org/wiki/Canonical\\_correlation](https://en.wikipedia.org/wiki/Canonical_correlation)
- [30] Hotelling, H. (1992) Relations between Two Sets of Variates. In: *Breakthroughs in Statistics*, Springer, New York, 162-190. [https://doi.org/10.1007/978-1-4612-4380-9\\_14](https://doi.org/10.1007/978-1-4612-4380-9_14)
- [31] Rayleigh Quotient. [https://en.wikipedia.org/wiki/Rayleigh\\_quotient](https://en.wikipedia.org/wiki/Rayleigh_quotient)
- [32] Horn, R.A. and Johnson, C.A. (1985) Matrix Analysis. Cambridge University Press, Cambridge, 176-180. <https://doi.org/10.1017/CBO9780511810817>
- [33] Arfken, G. (1985) Mathematical Methods for Physicists. 3rd Edition, Academic Press Inc., Cambridge, Chapter 4.6.
- [34] Carlin, H.J. and Giordano, A.B. (1964) Network Theory: An Introduction to Reciprocal and Non-Reciprocal Circuits. Prentice Hall, Upper Saddle River, Chapter 5.
- [35] Tellegen, B.D.H. (1948) The Gyrator, a New Electric Network Element. *Philips Research Reports*, **3**, 81-101.
- [36] Ausserlechner, U. (2016) A Method to Compute the Hall-Geometry Factor at Weak

Magnetic Field in Closed Analytical Form. *Electrical Engineering*, **98**, 189-206.

<https://doi.org/10.1007/s00202-015-0351-4>

- [37] Kellogg, O.D. (1954) *Foundations of Potential Theory*. Dover Publications Inc., New York, Chapter VIII, Section 6, Theorem X.
- [38] Carlin, H.J. and Giordano, A.B. (1964) *Network Theory: An Introduction to Reciprocal and Nonreciprocal Circuits*. Prentice-Hall, Upper Saddle River, Section 5.5, Figure 5.13 (c).

## Appendix A

**Figure A1** shows the symbol of a gyrator two-port and its defining equations [34]. Input voltage is linked to output current via a negative trans-resistance— $r$  and output voltage is linked to input current via a positive trans-resistance  $r$ . The arrow denotes the direction input to output. The sign inversion makes the gyrator a non-reciprocal device with odd symmetry of its resistance matrix.

$$\begin{pmatrix} V_1 \\ V_2 \end{pmatrix} = \begin{pmatrix} 0 & -r \\ r & 0 \end{pmatrix} \cdot \begin{pmatrix} I_1 \\ I_2 \end{pmatrix} \quad (\text{A1})$$

In spite of their trans-*resistance*, gyrators are lossless passive devices, which do not dissipate or generate or store electrical energy—their instantaneous power vanishes [35]

$$V_1 I_1 + V_2 I_2 = -r I_1 I_2 + r I_1 I_2 = 0 \quad (\text{A2})$$

These properties make gyrators similar to ideal transformers. In fact, gyrators are more basic than ideal transformers, because every ideal transformer is equivalent to a cascaded connection of two gyrators as is shown in **Figure A2**. This holds also for d.c. current.

It is possible to build up a gyrator by a parallel connection of two voltage-controlled current sources (VCCS)—one in forward direction and the other one in backward direction (see **Figure A3**). Alternatively one may use two current-controlled voltage sources (CCVS) instead of the two VCCS.

One widely known property of a gyrator is that it converts capacitances into inductances. If we connect a capacitor across the secondary port of the gyrator, it holds

$$V_2 = -I_2 \times \frac{1}{j\omega C} \quad (\text{A3})$$

whereby  $j$  is the imaginary unit,  $\omega$  the angular frequency, and  $C$  the capacitance. At the input port of the gyrator we have

$$V_1 = -r I_2 = j\omega C r V_2 = j\omega C r^2 I_1 \quad (\text{A4})$$

which is the impedance of an inductor with inductance equal to  $C \times r^2$ . It seems to be less known that this “inversion of resistance” property can also be used to convert an ampere-meter into a voltmeter, and vice versa. This is shown in **Figure A4**. With its zero resistance the ampere-meter shorts the output port of the gyrator. Due to (A1) this implies that the current at the input port of the gyrator vanishes, *i.e.*, the impedance at the input is infinite like for an ideal voltmeter. On the other hand, the voltage at the input port of the gyrator shows up as a current at the output port, where it is measured by the ampere-meter.

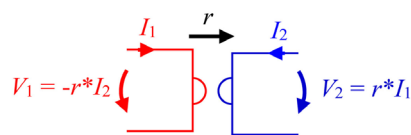


**Figure A1.** Symbol and defining equations of the gyrator.

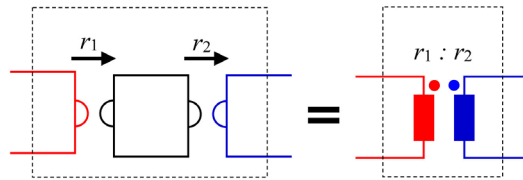


**Figure A2.** Two cascaded gyrators with trans-resistances  $r_1, r_2$  make an ideal transformer with turns ratio  $r_1:r_2$ .

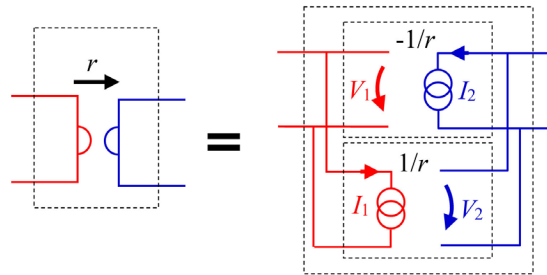


**Figure A3.** A gyrator consists of two anti-parallel voltage controlled current sources (VCCS) with trans-conductances of equal magnitude and opposite sign.

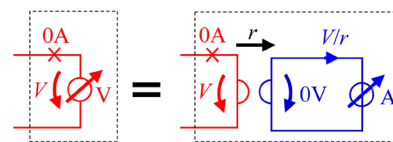


**Figure A4.** A voltmeter can be made by a gyrator working on an ammeter. The input resistance is infinite.

We make use of this property in hybrid operating modes of Hall plates for adding current and voltage signals. We could also have used simple trans-conductance amplifiers (OTAs), but they are (1) not passive (they provide arbitrarily large power when their output works on a high ohmic load), and (2) they are not bi-directional (which means that their output resistance is infinite and therefore we could not apply the theory of Nyquist and Johnson to compute the thermal noise at their output). This is the reason why we use gyrators in conceptual circuits like in **Figure 3**.

### Appendix B

Here we prove that  $X \cdot R + \bar{X}$  is non-singular. With  $X \cdot R + \bar{X} = (X + \bar{X} \cdot G) \cdot R$  it suffices to prove that  $X + \bar{X} \cdot G$  is non-singular. It is non-singular if it is positive definite, because then all its eigenvalues are positive.  $X + \bar{X} \cdot G$  is not symmetric. Hence, it is positive definite, if its symmetric part  $g = X + (\bar{X} \cdot G + G^T \cdot \bar{X})/2$  is positive definite. However, if the symmetric matrix  $g$  is positive definite, it can be interpreted as the conductance matrix of a resistor network. The opposite also holds: if we can find a resistor network whose conductance matrix is  $g$  then we know it must be positive definite, because the conductance matrix of passive dissipative networks is positive definite (because any excitation with non-vanishing voltage vectors  $V$  inevitably dissi-

pates power  $V^T \cdot g \cdot V > 0$ ).

Therefore we have to study, how  $g$  looks like. If we multiply  $G$  from left with  $\bar{X}$  we sieve out all rows of  $G$  where  $\bar{X}$  is 0 on the main diagonal. The exemplary case of  $N = 5$  and  $x = 6$  gives

$$\bar{X} \cdot G = \begin{pmatrix} 1 & 0 & 0 & 0 \\ 0 & 0 & 0 & 0 \\ 0 & 0 & 0 & 0 \\ 0 & 0 & 0 & 1 \end{pmatrix} \cdot \begin{pmatrix} G_{11} & G_{12} & G_{13} & G_{14} \\ G_{21} & G_{22} & G_{23} & G_{24} \\ G_{31} & G_{32} & G_{33} & G_{34} \\ G_{41} & G_{42} & G_{43} & G_{44} \end{pmatrix} = \begin{pmatrix} G_{11} & G_{12} & G_{13} & G_{14} \\ 0 & 0 & 0 & 0 \\ 0 & 0 & 0 & 0 \\ G_{41} & G_{42} & G_{43} & G_{44} \end{pmatrix} \quad (B1)$$

If we multiply  $G^T$  from right with  $\bar{X}$  we sieve out all columns of  $G^T$  where  $\bar{X}$  is 0 on the main diagonal.

$$G^T \cdot \bar{X} = \begin{pmatrix} G_{11} & G_{12} & G_{13} & G_{14} \\ G_{21} & G_{22} & G_{23} & G_{24} \\ G_{31} & G_{32} & G_{33} & G_{34} \\ G_{41} & G_{42} & G_{43} & G_{44} \end{pmatrix} \cdot \begin{pmatrix} 1 & 0 & 0 & 0 \\ 0 & 0 & 0 & 0 \\ 0 & 0 & 0 & 0 \\ 0 & 0 & 0 & 1 \end{pmatrix} = \begin{pmatrix} G_{11} & 0 & 0 & G_{41} \\ G_{12} & 0 & 0 & G_{42} \\ G_{13} & 0 & 0 & G_{43} \\ G_{41} & 0 & 0 & G_{44} \end{pmatrix} \quad (B2)$$

In this example we get

$$g = X + \frac{\bar{X} \cdot G + G^T \cdot \bar{X}}{2} = \begin{pmatrix} 0 & 0 & 0 & 0 \\ 0 & 1 & 0 & 0 \\ 0 & 0 & 1 & 0 \\ 0 & 0 & 0 & 0 \end{pmatrix} + \frac{1}{2} \begin{pmatrix} G_{11} & G_{12} & G_{13} & G_{14} \\ 0 & 0 & 0 & 0 \\ 0 & 0 & 0 & 0 \\ G_{41} & G_{42} & G_{43} & G_{44} \end{pmatrix} + \frac{1}{2} \begin{pmatrix} G_{11} & 0 & 0 & G_{41} \\ G_{12} & 0 & 0 & G_{42} \\ G_{13} & 0 & 0 & G_{43} \\ G_{41} & 0 & 0 & G_{44} \end{pmatrix} \quad (B3)$$

$$= \begin{pmatrix} G_{11} & G_{12}/2 & G_{13}/2 & (G_{14} + G_{41})/2 \\ G_{12}/2 & 1 & 0 & G_{42}/2 \\ G_{13}/2 & 0 & 1 & G_{43}/2 \\ (G_{14} + G_{41})/2 & G_{42}/2 & G_{43}/2 & G_{44} \end{pmatrix}$$

Hence, we see that  $g$  has on the main diagonal either 1 or  $G_{kk}$ , and the off-diagonal entries are 0,  $G_{km}/2$ , or  $(G_{km} + G_{mk})/2$ . Since the conductance matrix  $G$  of the Hall plate is positive definite, it holds  $G_{kk} > 0$ . Moreover,  $G_{km} < 0$  for  $k \neq m$  (which we prove below). Thus, the matrix  $g$  has positive entries on the main diagonal and negative or zero entries off the main diagonal. Therefore it represents the conductance matrix of a resistor network with resistors having positive resistance values. **Figure B1** shows the resistor network in the case of our example in (B3). Therefore  $g$  is positive definite and consequently the inverse of  $X \cdot R + \bar{X}$  exists.

Finally we prove that the off-diagonal terms in the matrix  $G$  of a Hall plate are negative, irrespective of the magnetic field. To this end we consider the operating condition of the Hall plate in **Figure B2**. A voltage source  $V_m > 0$  is connected to contact  $m$  while all other contacts are grounded. Then the current  $I_k$  into contact  $k$  is given by  $I_k = G_{km} V_m$ . We have to prove that this current is negative, because then it follows  $G_{km} < 0$ .

The electric field in the Hall plate can be expressed as the negative gradient of the electric potential. This potential is harmonic in the closed bounded region of

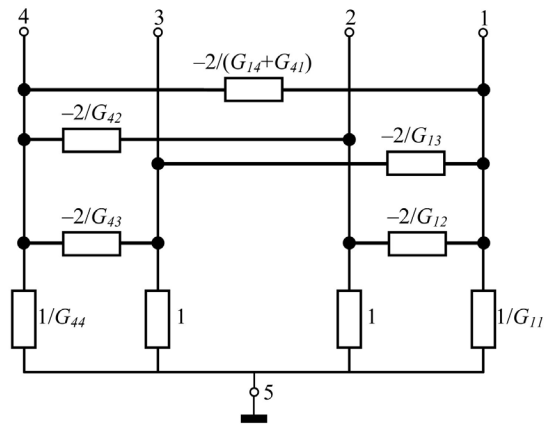


**Figure B1.** Example of a resistor network with five terminals having the conductance matrix from (B3). All resistance values are positive. There is no resistance between terminals 2 and 3, because  $g_{23} = 0$ .

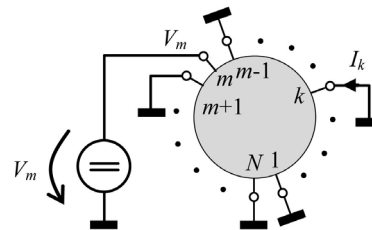


**Figure B2.** Definition of  $G_{km}$  of a Hall plate at arbitrary magnetic field. Potential  $V_m$  is applied to contact  $m$  and all other contacts are grounded. For  $V_m > 0$  it follows  $I_k < 0$ . Therefore  $G_{km} < 0$  for  $k \neq m$ .

the Hall plate, *i.e.*, it satisfies Laplace’s equation in the interior and it is continuous in the interior and on the boundary (see [36]). According to basic potential theory [37], a harmonic function attains its maximum and minimum values only on the boundary (if we rule out the trivial case of homogeneous potential in the Hall plate). The case of minimum potential on the boundary is drawn in **Figure B3** (see also Figure 5.13 in [38]). There, the negative supply contact  $k$  is shown with iso-potential lines and electric field lines. The electric field is perpendicular on the isopotential lines and on the perfectly conducting contact. The current density is not parallel to the electric field, because there is the Hall angle between both vectors. However, since the Hall angle is smaller than  $90^\circ$ , the current density has a non-vanishing component in the direction of the electric field. Integrating this normal component of the current density over the contact gives the current, which flows from the Hall interior through the contact against ground. Thus, we have proven that current flows out of contact  $k$  towards ground irrespective of the Hall angle, *i.e.*, irrespective of the applied magnetic field. In this derivation we have implicitly assumed a *contact* in the location of the minimum potential along the boundary. The discussion shows that there *must* be a contact to deliver the current—in other words, the maximum and minimum potentials on the boundary cannot occur on the insulating boundary.

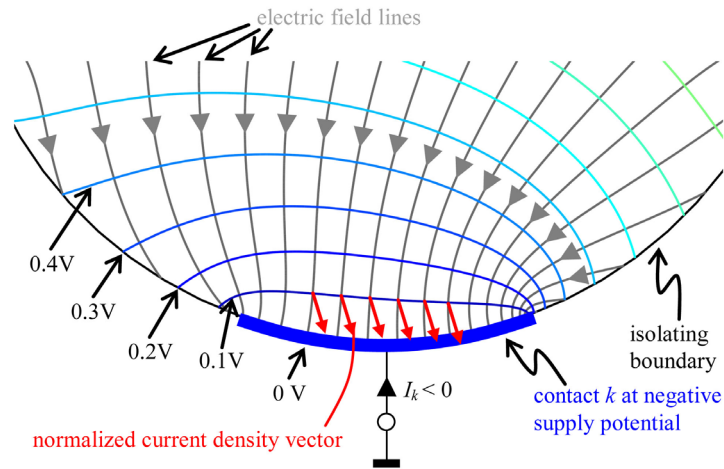


**Figure B3.** Current density vectors, electric field lines, and isopotential lines near the negative supply contact of a Hall plate at strong magnetic field (22.5° Hall angle).

### Appendix C

Here we prove the following symmetry properties of the hybrid matrices (hybrid reverse magnetic field reciprocity HRMFR).

$$\mathbf{H}^{(x)}(-B_{\perp}) = (\mathbf{X} - \bar{\mathbf{X}}) \cdot (\mathbf{H}^{(x)})^T \cdot (\mathbf{X} - \bar{\mathbf{X}}) \tag{C1a}$$

$$(\mathbf{H}^{(x)})^T = (\mathbf{X} - \bar{\mathbf{X}}) \cdot \mathbf{H}^{(x)}(-B_{\perp}) \cdot (\mathbf{X} - \bar{\mathbf{X}}) \tag{C1b}$$

(C1a) follows from (C1b) because the diagonal elements of the diagonal matrix  $\mathbf{X} - \bar{\mathbf{X}}$  can have only one of the two values  $\pm 1$ , and the matrix is identical to its inverse (21e).

$$(\mathbf{X} - \bar{\mathbf{X}}) \cdot (\mathbf{X} - \bar{\mathbf{X}}) = \mathbf{X} - \mathbf{X}\bar{\mathbf{X}} - \bar{\mathbf{X}}\mathbf{X} + \bar{\mathbf{X}} = \mathbf{X} + \bar{\mathbf{X}} = \mathbf{I} \tag{C2}$$

In (C2) we used (21d). We prove (C1b) by inserting (26c), which gives

$$(\mathbf{H}^{(x)})^T = (\mathbf{X} - \bar{\mathbf{X}}) \cdot (\bar{\mathbf{X}} \cdot \mathbf{R}^T + \mathbf{X}) \cdot (\mathbf{X} \cdot \mathbf{R}^T + \bar{\mathbf{X}})^{-1} \cdot (\mathbf{X} - \bar{\mathbf{X}}) \tag{C3}$$

In (C3) we expand the first two terms at the RHS and also the left two terms at the RHS, respectively, whereby we use (21c), (21d), and (C2).

$$(\mathbf{H}^{(x)})^T = (\mathbf{X} - \bar{\mathbf{X}} \cdot \mathbf{R}^T) \cdot (\mathbf{X} \cdot \mathbf{R}^T - \bar{\mathbf{X}})^{-1} \tag{C4}$$

We set the transpose of (C4) equal to (26a).

$$(\mathbf{R} \cdot \mathbf{X} - \bar{\mathbf{X}})^{-1} \cdot (\mathbf{X} - \mathbf{R} \cdot \bar{\mathbf{X}}) = (\bar{\mathbf{X}} \cdot \mathbf{R} + \mathbf{X}) \cdot (\mathbf{X} \cdot \mathbf{R} + \bar{\mathbf{X}})^{-1} \tag{D5}$$

(D5) is equal to

$$(\mathbf{X} - \mathbf{R} \cdot \bar{\mathbf{X}}) \cdot (\mathbf{X} \cdot \mathbf{R} + \bar{\mathbf{X}}) = (\mathbf{R} \cdot \mathbf{X} - \bar{\mathbf{X}}) \cdot (\bar{\mathbf{X}} \cdot \mathbf{R} + \mathbf{X}) \tag{D6}$$

We expand (C6) and use again (21c) and (21d).

$$\mathbf{X} \cdot \mathbf{R} - \mathbf{R} \cdot \bar{\mathbf{X}} = \mathbf{R} \cdot \mathbf{X} - \bar{\mathbf{X}} \cdot \mathbf{R} \tag{C7}$$

Finally we eliminate  $\bar{\mathbf{X}}$  in (C7) with (21b) to show the identity of both sides of (C7).

$$\mathbf{X} \cdot \mathbf{R} - \mathbf{R} + \mathbf{R} \cdot \mathbf{X} = \mathbf{R} \cdot \mathbf{X} - \mathbf{R} + \mathbf{X} \cdot \mathbf{R} \tag{C8}$$

The proof goes in the reverse direction: it starts with (C8) and goes via (C7), (C6), ... to (C3), and it ends with (C1b). From (C1b) the following relations follow

$$\mathbf{X} \cdot \left(\mathbf{H}^{(x)}\right)^{\top} \cdot \mathbf{X} = \mathbf{X} \cdot \mathbf{H}^{(x)}(-B_{\perp}) \cdot \mathbf{X} \tag{C9a}$$

$$\bar{\mathbf{X}} \cdot \left(\mathbf{H}^{(x)}\right)^{\top} \cdot \bar{\mathbf{X}} = \bar{\mathbf{X}} \cdot \mathbf{H}^{(x)}(-B_{\perp}) \cdot \bar{\mathbf{X}} \tag{C9b}$$

$$\mathbf{X} \cdot \left(\mathbf{H}^{(x)}\right)^{\top} \cdot \bar{\mathbf{X}} = -\mathbf{X} \cdot \mathbf{H}^{(x)}(-B_{\perp}) \cdot \bar{\mathbf{X}} \tag{C9c}$$

$$\bar{\mathbf{X}} \cdot \left(\mathbf{H}^{(z)}\right)^{\top} \cdot \mathbf{X} = -\bar{\mathbf{X}} \cdot \mathbf{H}^{(z)}(-B_{\perp}) \cdot \mathbf{X} \tag{C9d}$$

If we add (C9a-d) we get again (C1a). The operation  $\mathbf{Y} = \mathbf{X} \cdot \mathbf{M} \cdot \mathbf{X}$  on a matrix  $\mathbf{M}$  generates a new matrix  $\mathbf{Y}$ , whereby  $Y_{m,k}$  is unchanged if elements  $m$  and  $k$  on the diagonal of  $\mathbf{X}$  are equal to 1; all other elements of  $\mathbf{Y}$  vanish. In other words the operation  $\mathbf{X} \cdot \mathbf{M} \cdot \mathbf{X}$  acts like a sieve that lets pass only those elements of  $\mathbf{M}$  which are at the crossings of rows and columns, where the bit pattern of  $x_{\text{bin}}$  has 1-s. Analogous interpretations hold for the operations in (C9b-d). Therefore, we can decompose any matrix  $\mathbf{M}$  like this

$$\begin{aligned} \mathbf{M} &= (\mathbf{X} + \bar{\mathbf{X}}) \cdot \mathbf{M} \cdot (\mathbf{X} + \bar{\mathbf{X}}) \\ &= \mathbf{X} \cdot \mathbf{M} \cdot \mathbf{X} + \bar{\mathbf{X}} \cdot \mathbf{M} \cdot \bar{\mathbf{X}} + \bar{\mathbf{X}} \cdot \mathbf{M} \cdot \mathbf{X} + \mathbf{X} \cdot \mathbf{M} \cdot \bar{\mathbf{X}} \end{aligned} \tag{C10}$$

### Appendix D

Here we prove (47), which reads in its long version like this

$$\left[ \left( \bar{\mathbf{X}} - \mathbf{X} \cdot \left(\mathbf{H}_0^{(x)}\right)^{\top} \right) \cdot \left( \left(\mathbf{H}_0^{(x)}\right)^{-1} \cdot \bar{\mathbf{X}} - \mathbf{X} \right) \right]^{-1} = \mathbf{R}_0 \cdot \bar{\mathbf{X}} + \mathbf{X} \cdot \mathbf{R}_0 \tag{D1}$$

(D1) is identical to

$$\begin{aligned} \mathbf{1} &= \left( \bar{\mathbf{X}} - \mathbf{X} \cdot \left(\mathbf{H}_0^{(x)}\right)^{\top} \right) \cdot \left( \left(\mathbf{H}_0^{(x)}\right)^{-1} \cdot \bar{\mathbf{X}} - \mathbf{X} \right) \cdot \mathbf{R}_0 \cdot \bar{\mathbf{X}} \\ &\quad + \left( \bar{\mathbf{X}} - \mathbf{X} \cdot \left(\mathbf{H}_0^{(x)}\right)^{\top} \right) \cdot \left( \left(\mathbf{H}_0^{(x)}\right)^{-1} \cdot \bar{\mathbf{X}} - \mathbf{X} \right) \cdot \mathbf{X} \cdot \mathbf{R}_0 \end{aligned} \tag{D2}$$

Using (24) in (26a) gives

$$\left(\mathbf{H}_0^{(x)}\right)^{-1} \cdot (\bar{\mathbf{X}} \cdot \mathbf{R}_0 + \mathbf{X}) = (\mathbf{X} \cdot \mathbf{R}_0 + \bar{\mathbf{X}}) \tag{D3}$$

Rearranging (D3) gives

$$\left( \left(\mathbf{H}_0^{(x)}\right)^{-1} \cdot \bar{\mathbf{X}} - \mathbf{X} \right) \cdot \mathbf{R}_0 = \bar{\mathbf{X}} - \left(\mathbf{H}_0^{(x)}\right)^{-1} \cdot \mathbf{X} \tag{D4}$$

Plugging (D4) into (D2) gives

$$\begin{aligned} \mathbf{1} &= \left( \bar{\mathbf{X}} - \mathbf{X} \cdot \left(\mathbf{H}_0^{(x)}\right)^{\top} \right) \cdot \left( \bar{\mathbf{X}} - \left(\mathbf{H}_0^{(x)}\right)^{-1} \cdot \mathbf{X} \right) \cdot \bar{\mathbf{X}} \\ &\quad + \left( \bar{\mathbf{X}} - \mathbf{X} \cdot \left(\mathbf{H}_0^{(x)}\right)^{\top} \right) \cdot \left( \left(\mathbf{H}_0^{(x)}\right)^{-1} \cdot \bar{\mathbf{X}} - \mathbf{X} \right) \cdot \mathbf{X} \cdot \mathbf{R}_0 \end{aligned} \tag{D5}$$

Using (21c) in (D5) gives

$$\mathbf{1} = \left( \bar{X} - X \cdot \left( H_0^{(x)} \right)^\top \right) \cdot \bar{X} - \left( \bar{X} - X \cdot \left( H_0^{(x)} \right)^\top \right) \cdot X \cdot R_0 \quad (\text{D6})$$

From (36b) we get

$$X \cdot \left( H_0^{(x)} \right)^\top = X \cdot H_0^{(x)} \cdot (X - \bar{X}) \quad (\text{D7})$$

Inserting (D7) into (D6) gives

$$\begin{aligned} \mathbf{1} &= \left( \bar{X} - X \cdot H_0^{(x)} \cdot (X - \bar{X}) \right) \cdot \bar{X} - \left( \bar{X} - X \cdot H_0^{(x)} \cdot (X - \bar{X}) \right) \cdot X \cdot R_0 \\ &= \bar{X} + X \cdot H_0^{(x)} \cdot \bar{X} + X \cdot H_0^{(x)} \cdot X \cdot R_0 \\ &= \bar{X} + X \cdot H_0^{(x)} \cdot (\bar{X} + X \cdot R_0) \end{aligned} \quad (\text{D8})$$

Plugging (38a) into (D8) gives

$$\mathbf{1} = \bar{X} + X \cdot (\bar{X} \cdot R_0 + X) = \bar{X} + X = \mathbf{1} \quad (\text{D9})$$

which immediately shows the identity.